CDF 8171
version 1

A Search for Narrow di-Muon Resonances

Michael Schmitt, Jeff Kaplan & Jane Nachtman

April 19, 2006

Abstract

We present a new search for narrow di-muon resonances in the CDF Run II data. Our method is new, relying only on an *a priori* parametrization of the di-muon continuum to test for the presence of new resonances. We assume that the width of any new resonance is small compared to the mass resolution, which is already quite good at CDF: $\sigma_M/M^2 \approx 2 \times 10^{-4}$. We have applied this method to data taken with the SUSY di-lepton trigger, corresponding to a luminosity of approximately 195 pb^{-1}. There is no evidence for any new resonances over the range $4 < M_{\mu\mu} < 200$ GeV, and so we have derived limits on the cross section, using the Feldman-Cousins prescription.

Contents

1 Motivation

There are three basic motivations to look for a narrow resonance in the di-muon data:

1. The data are there. We are obliged to explore them!
2. Evidence for a new resonance at $M_{\mu\mu} = 7.25$ GeV was found in the Run I data [1]. We must check this with Run II data.
3. There are many theoretical motivations for one or more extra gauge bosons which will decay into lepton pairs. There are other hypothetical objects which can produce a narrow peak in the di-muon mass spectrum as well. It is useful to test these speculations in an inclusive manner.

It also true that historic discoveries have been made in di-muon channels, such as the discovery of the Υ resonance [2].

Our approach is purely "data-driven" – we do not involve any theoretical models in any of our work. When we obtain a cross section measurement or limit, we assume that the acceptance for any narrow resonances is the same as for the Drell-Yan di-muon production at that same mass.

2 Method

The goal is to identify a narrow peak on top of a smooth continuum. Usually this is done by filling a histogram and scanning for a peak. We can avoid the difficulties and arbitrariness of binning by performing an unbinned likelihood fit to all the events in a given mass range. If some parametrization $B(x)$ of the continuum exists, and we know *a priori* the resolution $\sigma(x)$ on the mass x, then we can define the probability density simply as

$$\mathcal{P}(x; a) = a\, G(x) + (1 - a)\, B(x) \tag{1}$$

where $G(x)$ represents the shape of the signal, and the "amplitude" a is the only free parameter. For our analysis, we take $G(x)$ to be a Gaussian with width $\sigma(x)$, but of course any shape could be used that is sufficiently narrow compared to the range $x_{\rm LO} < x < x_{\rm HI}$. Necessarily, $G(x)$ and $B(x)$ are both normalized to unity when integrated over this range. We allow a to be non-positive as it must sometimes be in order to accommodate the data in the absence of a signal. As is customary and convenient, we work with the negative log-likelihood, $F \equiv -\ln \mathcal{P}$.

If a peak is present at $x = x_{\rm PK}$, then the minimization of $F(x_{\rm PK}, a)$ with respect to a will give us the "best" value for the amplitude, $a_{\rm BEST}$. We can expect that

1. $\Delta F(x_{\rm PK}, a_{\rm BEST}) \equiv F(x_{\rm PK}, a_{\rm BEST}) - F(x_{\rm PK}, 0)$ will be very different from zero (and negative, of course), and

2. the best amplitude is positive, $a_{\rm BEST} > 0$.

Equivalently, one can say that $a_{\rm BEST}$ will be positive and significantly different from zero, where the uncertainty on the amplitude, σ_a, is determined by the shape of $F(x_{\rm PK}, a)$ near $a = a_{\rm BEST}$.

We want to test for the presence of a peak anywhere in the range $x_{\rm LO} < x < x_{\rm HI}$. Our procedure, then, is to scan this range in steps of $\Delta x \sim \sigma(x)$, and at each value of x, find $a_{\rm BEST}$ and calculate ΔF. We hope to see, at one particular point $x_{\rm PK}$, a deep minimum in ΔF and a positive $a_{\rm BEST}$. In that case, the number of signal events will be $a_{\rm BEST} \times N_{\rm tot}$, where $N_{\rm tot}$ is the total number of events in the given range.

If we see evidence for a peak, then we must evaluate its significance, taking into account the fact that we have made a scan in small steps Δx across the range $x_{\rm LO} < x < x_{\rm HI}$. Since the continuum must give us small, insignificant peaks (and an equal number of negative contributions with $a_{\rm BEST} < 0$), a single positive $a_{\rm BEST}$ does not necessarily carry much significance. In other words, for a particular value of x, a value such as $\Delta F = -5^2/2 = -12.5$ does imply a significance of about "5σ" but since we have tried N values of x, this significance is diluted. In essence, we have pulled M values from a Gaussian distribution (for a), not one, so the probability to get a value at 5σ or higher is $M \times 5.7 \times 10^{-7}$. If the successive steps Δx are equal to $\sigma(x)$, then we find from toy Monte Carlo calculations that $M \approx N/4$.

If there is no evidence for a peak, then we need to set limits on the production of the peak, as a function of mass. Naively one could simply take the upper limit on the number of signal events to be $N_{\rm lim} = (a_{\rm BEST} + 1.96\sigma_a)N_{\rm tot}$, however, the fact that $a_{\rm BEST} < 0$ half the time means that sometimes $N_{\rm lim}$ can be negative, which is nonsense, physically. Fortunately, the Feldman-Cousins prescription [3] solves this problem for us. It also solves the problem of deciding when to switch from quoting an upper limit and when to report evidence for a signal; as they point out clearly in their article, the common practice of declaring "evidence" as soon as $a_{\rm BEST} > 3\sigma_a$ leads to statical under-coverage, which means that 95% confidence levels are less than 95% and 3σ evidence is not 3σ, etc. It is important to realize that the Feldman-Cousins prescription gives us a preferred range for the signal cross section (at some confidence level such as 95%), which may or may not include zero. We can expect that for some values of mass, this preferred range will not include zero due to upward fluctuations of the continuum. This does not mean that a signal is present, and typically zero signal will be excluded at a higher though still reasonable confidence level, if indeed no signal is present.

One of the nice features of this method is the escape from simulations; at no point do we need to know our sample composition. Of course, we do need to have a basic idea of what data we are analyzing, but the outcome of the scan does not depend on this in any quantitative

way. Furthermore, we will only need to know muon efficiencies, acceptance and luminosity in order to convert the number of signal events (or limits on the number of signal events) into a cross section. Thus, uncertainties on the background do not enter at all. We will remove the luminosity uncertainty and reduce the efficiency and acceptance uncertainties by normalizing our cross sections to that measured for the Z-boson resonance [4]. The estimation of the acceptance demands a model for the signal. We will assume that the acceptance for Drell-Yan events at a given mass is a good approximation for the signal acceptance. If the narrow resonance were produced in the decay of a more massive state, then the acceptance would probably be higher, since the muons would receive a higher transverse momentum from the decay of that state, particularly for lower di-muon masses, and they would be more centrally produced.

To recapitulate, this method relies on the following assumptions:

1. the continuum $B(x)$ can be parametrized in a simple manner across the range $x_{\rm LO} < x < x_{\rm HI}$; and,
2. the signal $G(x)$ is narrower than the mass resolution, and the total number of signal events is small compared to the total number of events.

In this sense the search is entirely data-driven, and is keyed to the *shape* of the observed distribution.

The first assumption will fail when we go to very high masses where the data become too sparse to allow for a simple parametrization. In this case one could rely on simulations. Instead, we have developed a different procedure which still focuses on the *shape* of the distribution. This method is described in Section 8.

3 Event Sample and Selection

The events are drawn from a sample of SUSY di-lepton events, and the event selection is very simple. We give details below.

3.1 Event Sample

Since we want to probe as wide a range of masses as possible, we cannot use the high-p_T inclusive muon sample. For the current analysis, we therefore turned to the SUSY di-lepton sample, which has relatively low p_T requirements for the muons.

According to the studies of the New Mexico group [5], the SUSY di-muon trigger demands the following:

- two muons both with $p_T > 4$ GeV
- the muons have stubs in one of these combinations: CMUP/CMUP, CMUP/CMX. (We ignore the cases of CMU-only muons, for now.)

We ran on most of the `edil0d` data sample, using good run list version 7 ("muon no Si"), for a luminosity of about 195 pb^{-1}.

3.2 Event Selection

The event selection is very simple. We demand:

- two good identified muons,
- they both must have $p_T > 5$ GeV,
- the muons must have opposite signs,
- their separation along the beamline is $|\Delta z_0| < 2$ cm,
- the event is not tagged as a comic ray.

We checked the bit for the level-3 SUSY di-muon trigger, also.

3.3 Muon Identification

Our muon identification is close to the standard "tight" cuts, except that we impose *sliding* cuts for the track-stub match and for the isolation, as described and justified in our earlier note Ref. [7]. We recapitulate the requirements here:

- track cuts
  1. $|z_0| < 60$ cm
  2. at least 3 axial and 2 stereo layers with ≥ 5 hits each
  3. $\chi^2/\text{dof} \leq 3$
  4. $|d_0| < 0.02$ cm if Silicon hits are present, 0.15 cm otherwise
- fiduciality requirement
  1. CMP: $x_{\text{fid}} < 0$ cm, $z_{\text{fid}} < -3$ cm, not bad blue-beam
  2. CMX: $x_{\text{fid}} < 0$ cm, $z_{\text{fid}} < -3$ cm, not bad keystone or miniskirt
  3. CMX: $\rho > 140$ cm
  4. (no CMU fiducial cuts)
- muon reconstruction
  1. require a stub linked with loose matching requirements
- muon ID cuts

	name	$x_{\rm LO}$ (GeV)	$x_{\rm HI}$ (GeV)	$N_{\rm tot}$
1	J/ψ	2.6	4.5	8102
2	4–9	3.8	9.1	2000
3	Υ	9	14	12349
4	13–84	13	84	8148
5	Z	80	120	3781
6	high	100	200	186
7	sparse	200	none	–

Table 1: *regions defined for scanning*

1. $E_{\rm em} < 2$ GeV or $E_{\rm em} < 2$ GeV $+ 0.0115(p - 100$ GeV) for $p > 100$ GeV
2. $E_{\rm had} < 6$ GeV or $E_{\rm had} < 6$ GeV $+ 0.028(p - 100$ GeV) for $p > 100$ GeV
3. matching cuts:
   (a) $|\Delta X_{\rm CMU}| < 6$ cm
   (b) $|\Delta X_{\rm CMP}| < \max(6\text{ cm}, 150/p_T)$
   (c) $|\Delta X_{\rm CMX}| < \max(6\text{ cm}, 125/p_T)$

- isolation

1. $I < \max(2\text{ GeV}, 0.1 \times p_T)$

4 Continuum Parameterizations

We need, first, a parametrization of the continuum, $B(x)$. Recognizing that there are several sets of known di-muon peaks, we divide the spectrum into six regions, as listed in Table 1, and parametrize each region individually. These regions overlap to a limited extent in order to avoid a compromised result at the extremes of each range. There is a seventh region, "sparse" which is not parametrized – see the discussion in Section 8.

Each of these regions needs to be described by an analytical function. We ignore the presence of any possible signal and provide Gaussians only for the known resonances. The choice of functions is arbitrary, and success is defined by examining the residuals with respect to parametrization for an appropriately binned histogram. The parameters for each function are set by minimizing an unbinned likelihood. For this we used a series of stand-alone programs with carefully optimized code; each region can be fit in a matter of seconds. In the subsections which follow, we give the details of the parameterizations and the fit. The parameters are listed with many significant figures in order to state exactly what was used for the scans discussed later.

4.1 The J/ψ Region

There are two visible peaks corresponding to the J/ψ and the ψ'. We use two Gaussians with a common mean for the J/ψ and a single Gaussian for the ψ'. The continuum under the peaks is described by a linear function. The complete likelihood is:

$$\mathcal{P}_1(x) = (1 - f_1 - f_2 - f_3)L(x) + f_1 G_1(x) + f_3 G_2(x) + f_3 G_3(x)$$

where the fractions f_1, f_2 and f_3 are to be determined by the minimization. The functions $L(x)$ and $G(x)$ are given by

$$\begin{aligned} L(x) &= \frac{A + Bx}{A(x_{\rm HI} - x_{\rm LO}) + B(x_{\rm HI}^2 - x_{\rm LO}^2)/2} \\ G(x) &= \frac{1}{\sqrt{2\pi}\,\sigma} \exp\left(-\frac{1}{2}\frac{(x-\mu)^2}{\sigma^2}\right) \end{aligned} \tag{2}$$

and integrate to unity over the range $x_{\rm LO} < x < x_{\rm HI}$. The minimization procedure leads to the following values:

$$\begin{aligned} A &= 0.709 \pm 0.027 \\ B &= -0.1150 \pm 0.0042 \\ \mu_1 = \mu_2 &= 3.08639 \pm 0.00050 \text{ GeV} \\ \sigma_1 &= 0.02380 \pm 0.00030 \text{ GeV} \\ \sigma_2 &= 0.0580 \pm 0.0014 \text{ GeV} \\ \mu_3 &= 3.67428 \pm 0.00197 \text{ GeV} \\ \sigma_3 &= 0.02860 \pm 0.00140 \text{ GeV} \\ f_1 &= 0.5460 \pm 0.0054 \\ f_2 &= 0.2205 \pm 0.0042 \\ f_3 &= 0.04790 \pm 0.00215 \end{aligned}$$

A comparison of this fit to the data is shown in Fig. 1, which shows a binned histogram with the fit superimposed, and also the absolute residuals. The fit is good.

4.2 The 4–9 Region

There are no known resonances in this region, so we fit the continuum to a second order polynomial:

$$\mathcal{P}_2(x) = \frac{A + B(x - C)^2}{A(x_{\rm HI} - x_{\rm LO}) + B[(x_{\rm HI} - C)^3 - (x_{\rm LO} - C)^3]/3}$$

where A, B and C are free parameters. Their values are:

$$\begin{aligned} A &= 20.990 \pm 4.29 \\ B &= 1.476 \pm 0.270 \\ C &= 6.403 \pm 0.110. \end{aligned}$$

A comparison of this fit to the data is shown in Fig. 2. The fit is good.

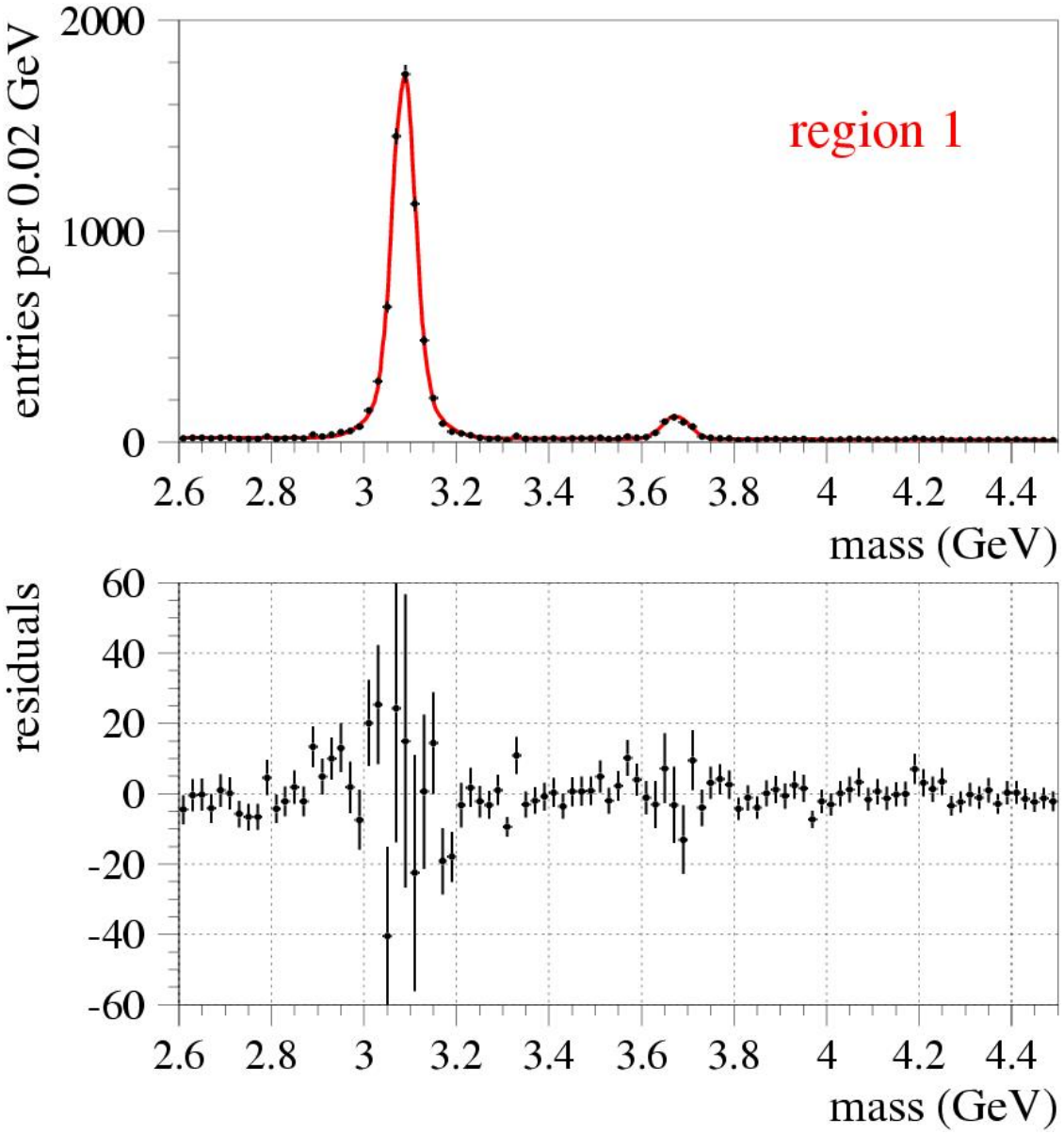

Figure 1: *fit to region 1. Top: binned histogram and the parametrization; Bottom: absolute residuals*

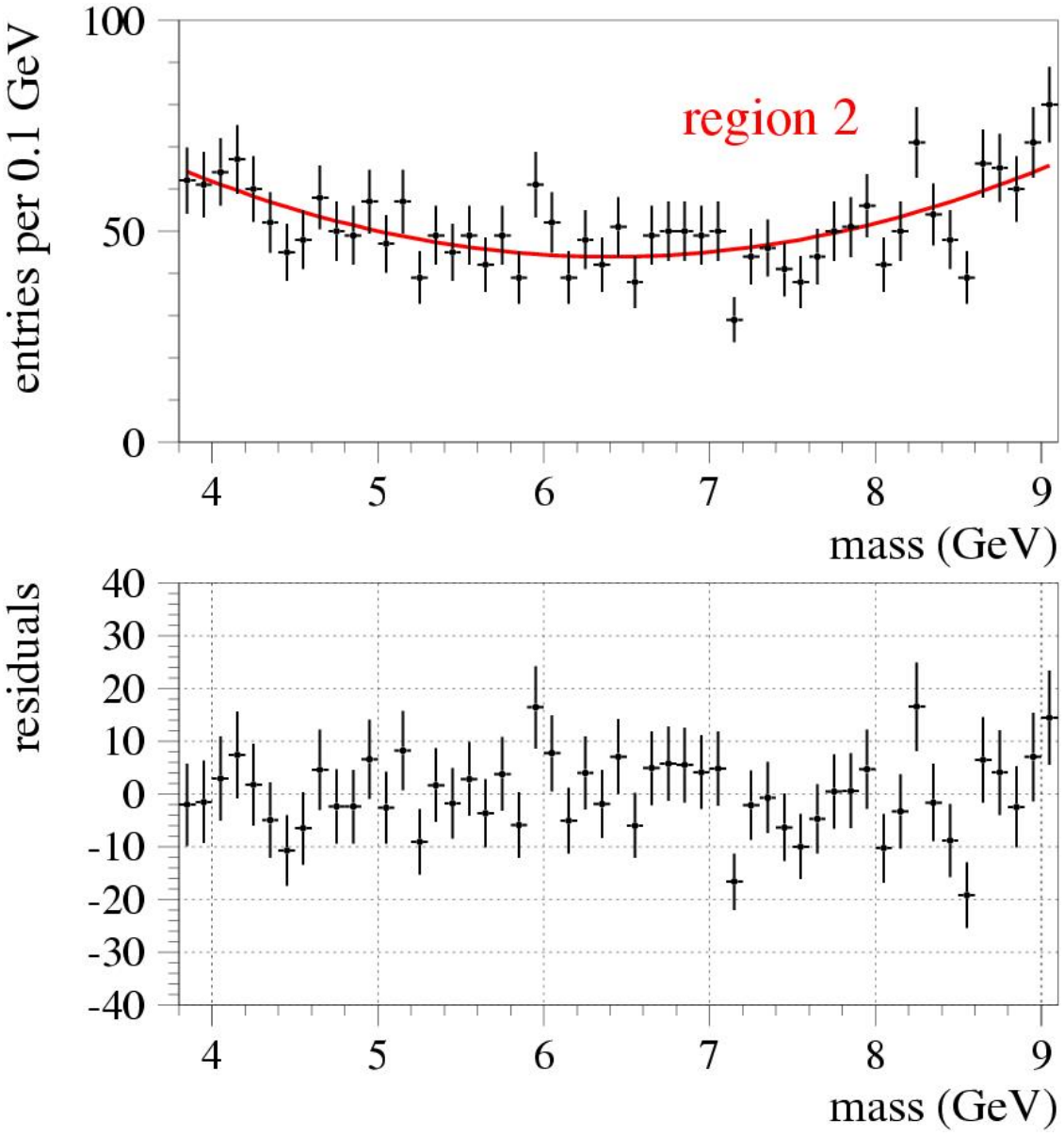

Figure 2: *fit to region 2. Top: binned histogram and the parametrization; Bottom: absolute residuals*

4.3 The Υ Region

This is the most complicated region. There are three distinct peaks, and also the continuum requires a second-order polynomial. We have fit a broad mass range above the Υ resonances in order to get a good handle on this continuum, and also to anchor the lower area of region 4, which is problematic due to the trigger threshold.

Our parametrization for this region is

$$\mathcal{P}_3(x) = (1 - f_1 - f_2 - f_3)Q(x) + f_1 G_1(x) + f_2 G_2(x) + f_3 G_3(x)$$

where $G(x)$ is defined in Eq. (2) and $Q(x)$ is defined by

$$Q(x) \equiv \frac{A + B(x - x_D) + C(x - x_D)^2}{A(x_{\rm HI} - x_{\rm LO}) + B[(x_{\rm HI} - x_D)^2 - (x_{\rm LO} - x_D)^2]/2 + C[(x_{\rm HI} - x_D)^3 - (x_{\rm LO} - x_D)^3]/3} \tag{3}$$

and $x_D \equiv 11.0$ GeV arbitrarily. This choice leads to smaller correlations among the parameters A, B and C. The parameter values are

$$\begin{aligned}
A &= 120.0 \pm 7.6 \\
B &= 18.40 \pm 0.70 \\
D &= -7.60 \pm 0.50 \\
\mu_1 &= 9.42912 \pm 0.00075 \text{ GeV} \\
\sigma_1 &= 0.0602 \pm 0.0007 \text{ GeV} \\
\mu_2 &= 9.99508 \pm 0.00189 \text{ GeV} \\
\sigma_2 &= 0.0562 \pm 0.0016 \text{ GeV} \\
\mu_3 &= 10.32526 \pm 0.00246 \text{ GeV} \\
\sigma_3 &= 0.05932 \pm 0.0020 \text{ GeV} \\
f_1 &= 0.2538 \pm 0.0036 \\
f_2 &= 0.1000 \pm 0.0018 \\
f_3 &= 0.07345 \pm 0.0016.
\end{aligned}$$

The fit is good, as can be seen from Fig. 3.

4.4 The 13–84 Region

We begin this parametrization well above the trigger threshold, so so this entire region benefits from an acceptance that rises relatively slowly – there is no sculpting of the dimuon p_T (q_T) distribution. This region extends up to the onset of the Z-resonance, and we describe this "toe" with a rising exponential. The likelihood function is, then,

$$\mathcal{P}_4(x) = (1 - f_1 - f_2)E_3(x) + f_1 E_1(x) + f_2 H(x)$$

where $E(x)$ and $H(x)$ are exponential functions:

$$E(x) = \frac{\exp(-x/\lambda)}{\lambda[\exp(-x_{\rm LO}/\lambda) - \exp(-x_{\rm HI}/\lambda)]}$$

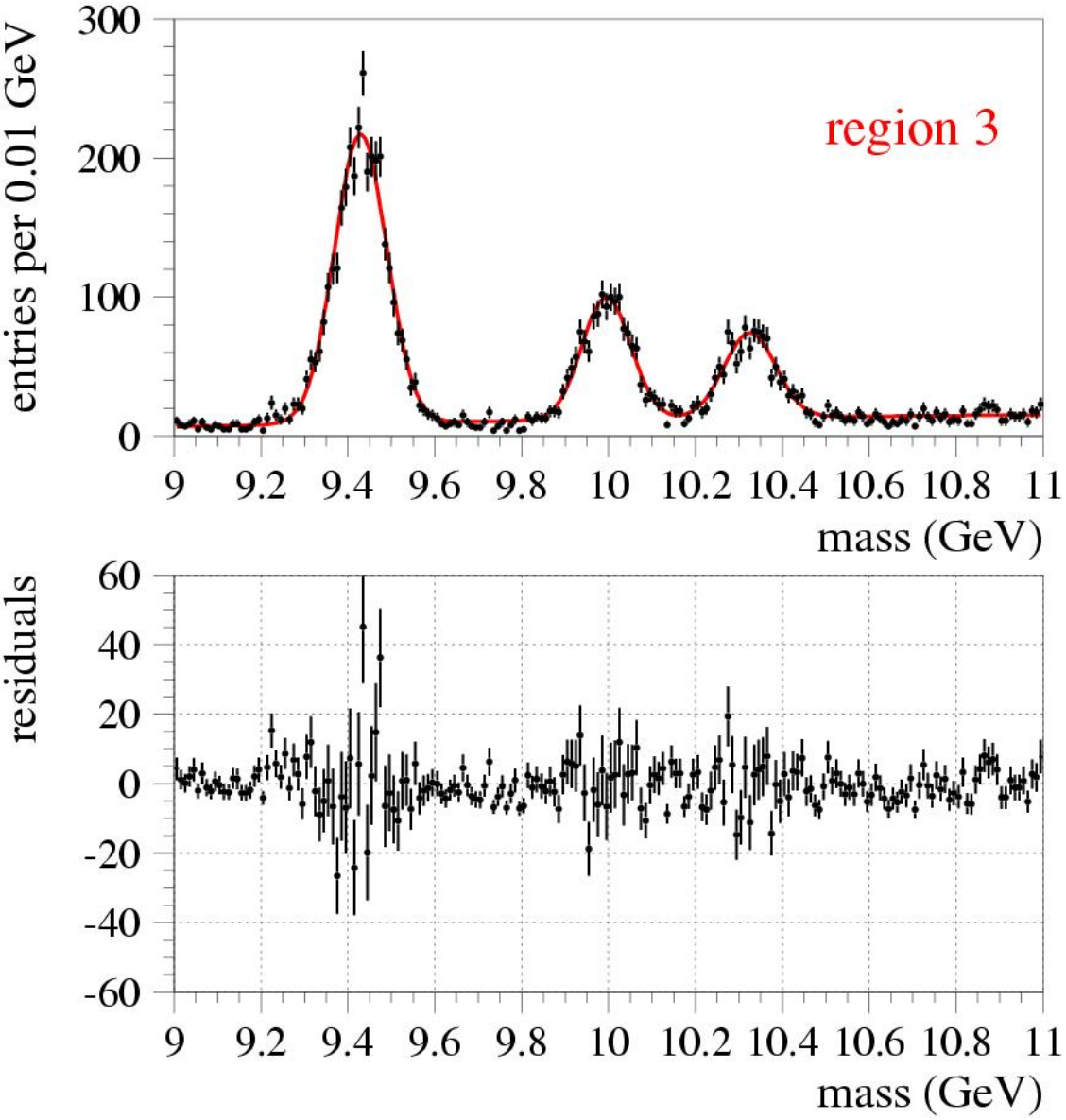

Figure 3: *fit to region 3. Top: binned histogram and the parametrization; Bottom: absolute residuals*

$$H(x) = \frac{\exp(-(x_{\rm HI}-x)/\lambda)}{\lambda\exp(-x_{\rm HI}/\lambda)[\exp(-x_{\rm HI}/\lambda)-\exp(-x_{\rm LO}/\lambda)]} \quad (4)$$

there are three λ parameters (λ_2 goes with $H(x)$). The parameter values are

$$\begin{aligned}
\lambda_1 &= 15.2025 \pm 0.416 \text{ GeV} \\
\lambda_2 &= 6.6015 \pm 0.7699 \text{ GeV} \\
\lambda_3 &= 3.5532 \pm 0.068 \text{ GeV} \\
f_1 &= 0.3050 \pm 0.0106 \\
f_2 &= 0.0350 \pm 0.018.
\end{aligned}$$

The quality of the fit can be gleaned from Fig. 4. Notice that the first couple of bins are *not* included in the fit, nor will we be scanning that region with this parametrization; rather, those bins are covered by the scan in the Υ region.

4.5 The Z-Peak Region

The Z-peak is not a simple Gaussian because the natural shape is really a Lorentzian, and also the mass resolution is not truly Gaussian. We parametrize this region with the sum of two Gaussians with a common center, and a linear function for the continuum:

$$\mathcal{P}_5(x) = (1-f_1-f_2)L(x) + f_1 G_1(x) + f_2 G_2(x)$$

where $L(x)$ and $G(x)$ are defined in Eq. (2). The parameter values are

$$\begin{aligned}
A &= 9.077 \pm 0.880 \\
B &= -0.210 \pm 0.040 \\
\mu &= 90.843 \pm 0.0048 \text{ GeV} \\
\sigma_1 &= 2.060 \pm 0.051 \text{ GeV} \\
\sigma_2 &= 5.140 \pm 0.212 \text{ GeV} \\
f_1 &= 0.577 \pm 0.007 \\
f_2 &= 0.327 \pm 0.008.
\end{aligned}$$

The comparison of this fit to the data is given in Fig. 5.

4.6 The High-Mass Region

The so-called "high-mass" region, which extends up to 200 GeV, has already been explored by previous analyses [6]. As far as we know, all the other regions have not been investigated in Run II. After some trial-and-error, we settled on the sum of two exponential functions to describe the continuum:

$$\mathcal{P}_6(x) = (1-f)E_1(x) + fE_2(x)$$

where $E(x)$ is already defined in Eq. (4). The parameters are:

$$\lambda_1 = 4.3006 \pm 0.7919 \text{ GeV}$$

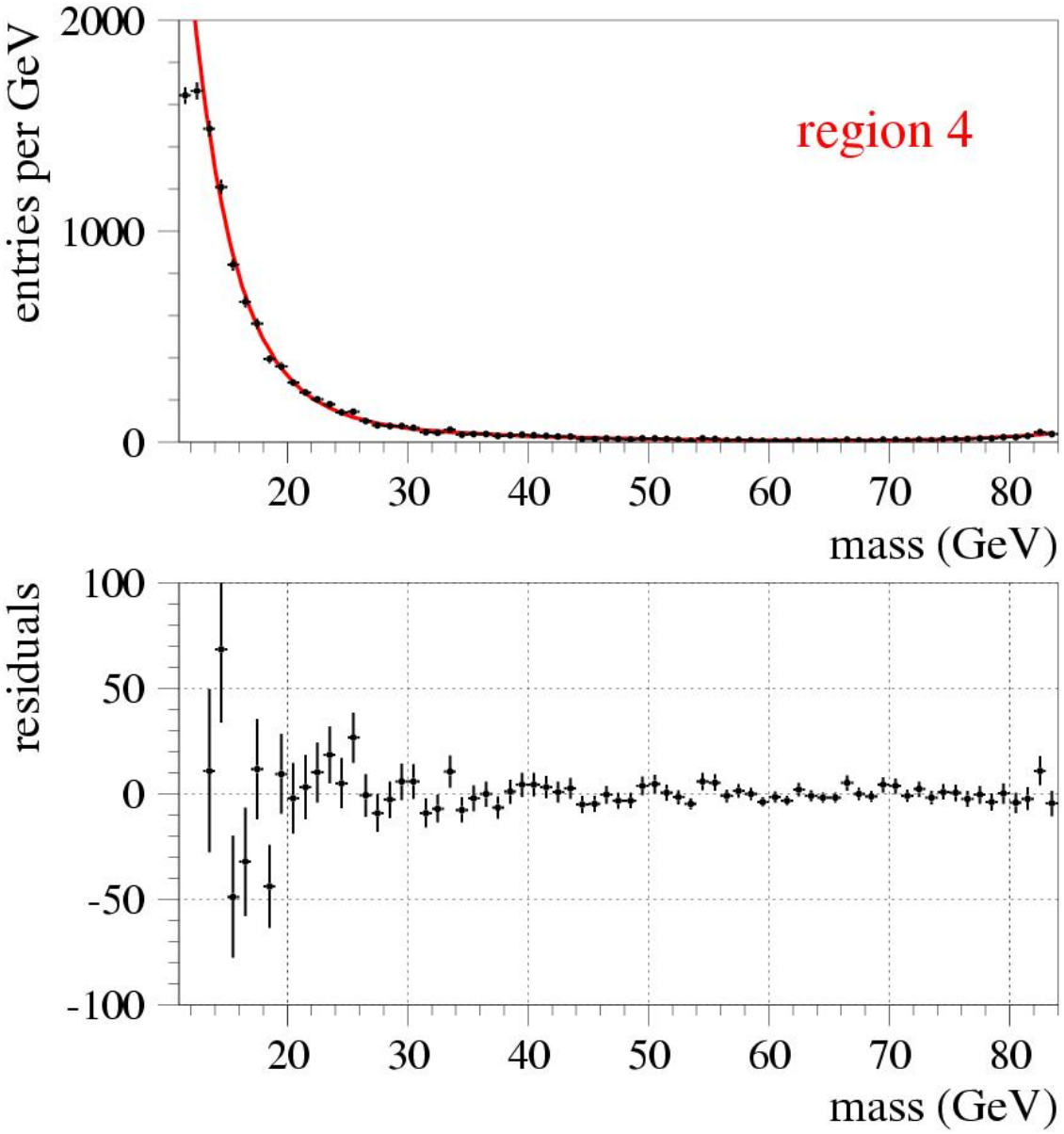

Figure 4: *fit to region 4. Top: binned histogram and the parametrization; Bottom: absolute residuals*

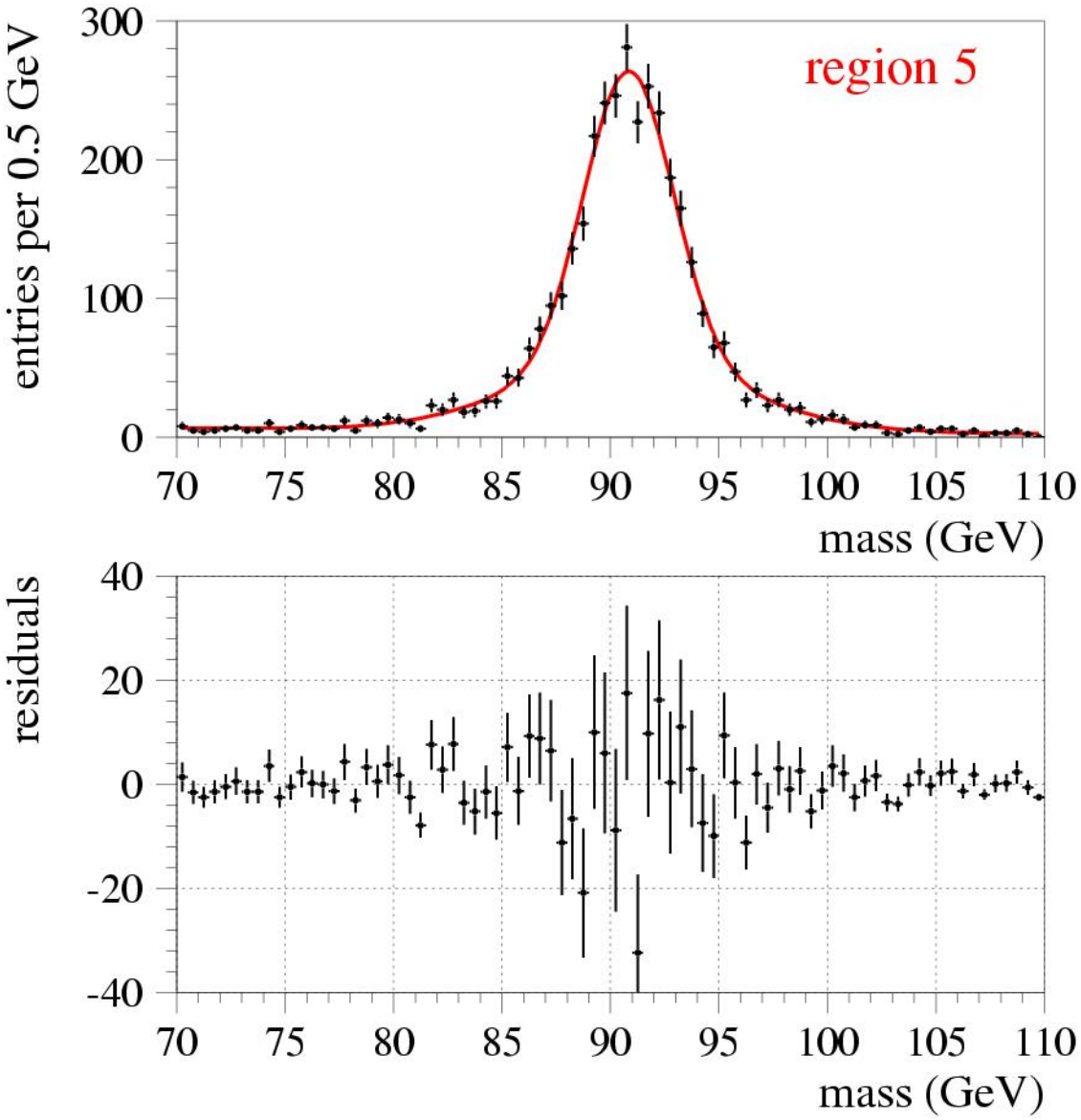

Figure 5: *fit to region 5. Top: binned histogram and the parametrization; Bottom: absolute residuals*

$$\begin{aligned} \lambda_2 &= 31.52 \pm 5.90 \text{ GeV} \\ f &= 0.4975 \pm 0.0530. \end{aligned}$$

The fit is compared to the binned data in Fig. 6.

5 The Scans

Given the parameterizations detailed in Sec. 4, we can proceed with the scan as described in Sec. 2.

We have chosen not to search for resonances in the J/ψ region as this region is well known already, and the "space" for peaks among the known resonances is quite small. We therefore tackle regions 2–6 and describe the results in the following subsections.

As pointed out before, these regions overlap somewhat in order to avoid gaps in the coverage. Due to the definition of the signal shape as a Gaussian as in Eq. (2), we cannot set the center of the Gaussian too close to $x_{\rm LO}$ or $x_{\rm HI}$ or the requirement that $G(x)$ be normalized to unity will not be met. In practice we begin the scan at $x_{\rm LO} + 2\sigma(x_{\rm LO})$ and end it at $x_{\rm HI} - 2\sigma(x_{\rm HI})$. For the sake of clarity, we designate the coverage of the mass range as follows:

mass range	region
4 – 9.05	2
9.05 – 13.5	3
13.5 – 82	4
82 – 105	5
105 – 200	6

This gives us full coverage from 4 GeV through 200 GeV. The region above 200 GeV is discussed separately in Sec. 8.

5.1 Signal Shape

We have taken a very simple view of the signal shape, ignoring details such as radiative tails or the tails in the p_T resolution function. These details would not be important if a clear signal were observed, nor will they have a large impact on the cross section limits when none is observed. An update with a more refined signal shape is always possible.

We do take into account the increase of the mass resolution with mass. For this we start with the studies done for another search project, the "sliding-q_T" search – see cdf note 7560 [7]. According to those studies, the mass resolution varies as

$$\frac{\sigma(x)}{x^2} = (1.6 \times 10^{-4}) + (1.4 \times 10^{-4}) \exp(-(x-20)/20) \tag{5}$$

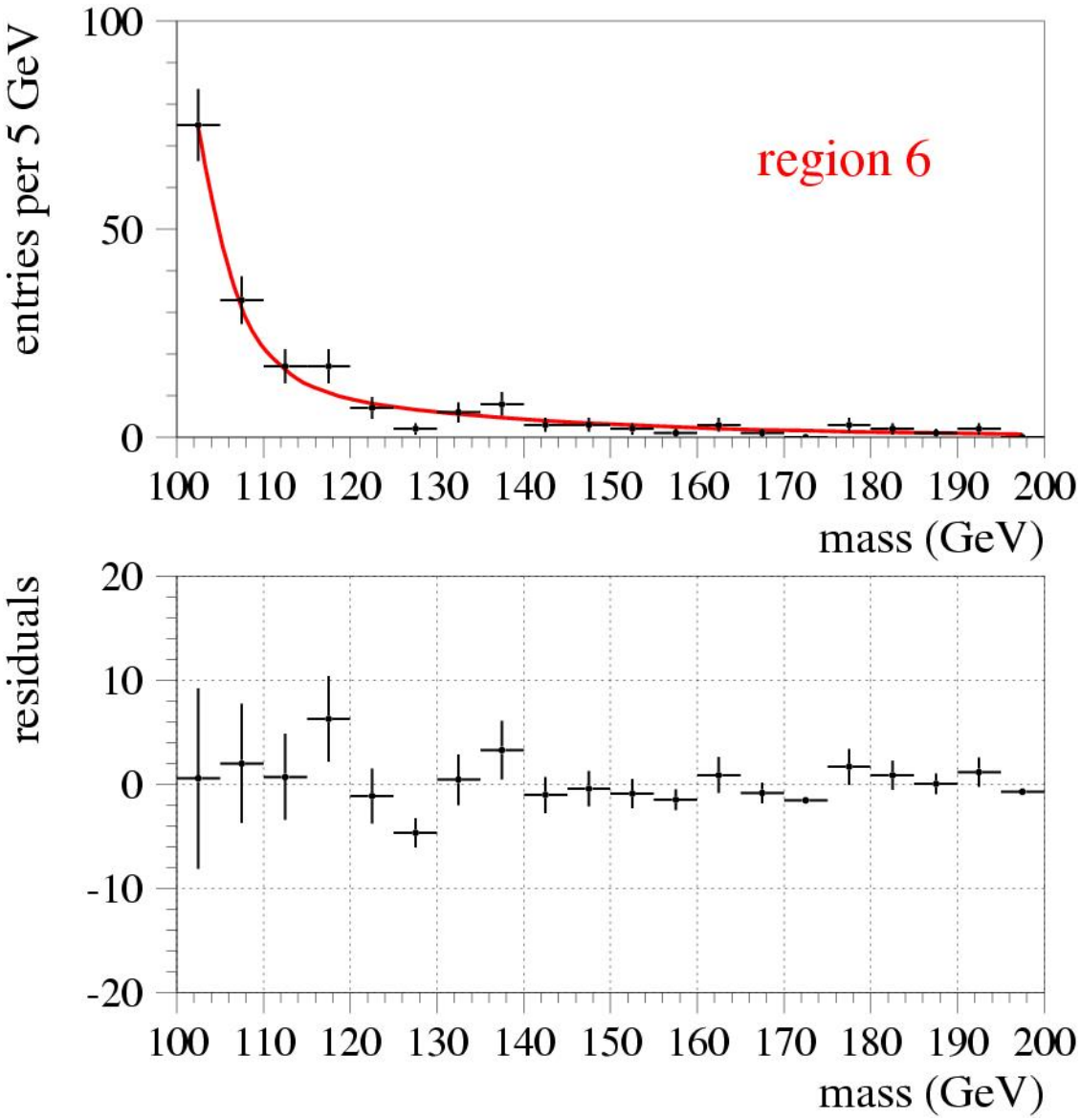

Figure 6: *fit to region 6. Top: binned histogram and the parametrization; Bottom: absolute residuals*

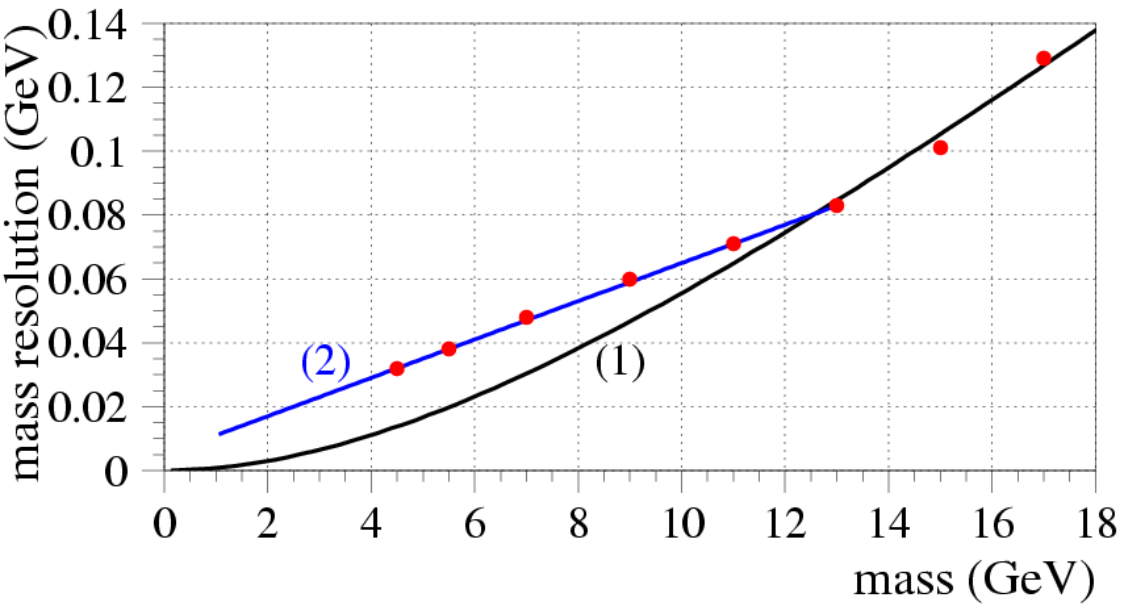

Figure 7: *measurement error on the mass as a function of true mass. Curve (1) corresponds to Eq. (5), which does not take into account the q_T bias of the event selection and hence underestimates the measurement errors at low masses. Curve (2) is an update which takes this q_T bias into account and is described by a straight-line fit as in Eq. (7).*

where x is in GeV.

This expression is appropriate for unbiased data, *i.e.*, for events with full acceptance as a function of q_T. Once we consider masses below the threshold defined by the $p_T > 5$ GeV requirement, however, the measurement error of the mass will be larger than that given by Eq. (5). We have addressed this effect in a generator-level study in which we apply the nominal kinematic and fiducial requirements to the muons, and then smear their momenta. We take the triple-Gaussian fit shown in Fig. 20 of cdf 7560 [7] and use it as the error function for the p_T of each muon. We scale the three Gaussian widths by a function which changes with mass:

$$\sigma_{p_T} \rightarrow \sigma_{p_T} \times (1 + \exp(-(p_T - 10)/6)) \tag{6}$$

which reproduces the behavior shown in Fig. 21 of cdf 7560 [7]. With this formula, we find a measurement error on the mass as a function of mass, as indicated by the dots in Fig. 7. Curve (1) represents formula Eq. (5) which clearly underestimates the error on the mass for $M_{\mu\mu} < 12$ GeV. The dots lie on a straight line given by curve (2) and parametrized by:

$$\sigma_M = 0.035 \text{ GeV} + 0.006 \times (M_{\mu\mu} - 5 \text{ GeV}). \tag{7}$$

We use this formula when setting the width of our signal peak as a function of mass, until the original formula in Eq. (5) takes over (*i.e.*, gives a larger value for σ_M).

For reference, we list here the mass resolutions obtained with these two formulas:

mass range (GeV)	assumed mass resolution (GeV)
4 – 9	0.029 – 0.059
9 – 13	0.059 – 0.085
13 – 84	0.085 – 1.20
84 – 110	1.20 – 1.97
110 – 200	1.97 – 6.40

We can make a comparison to the fitted widths of the known resonances as a cross-check:

resonance	fitted width (GeV)	assumed mass resolution (GeV)
J/ψ	0.024	0.024
ψ'	0.029	0.027
$\Upsilon(1s)$	0.060	0.061
$\Upsilon(2s)$	0.056	0.056
$\Upsilon(3s)$	0.059	0.059
Z	3.17	1.39

With the modification represented by Eq. (7), we obtain satisfactory agreement with the data for all of the low-lying resonances. The natural width of the Z-resonance contributes a lot to the fitted widths. The number 3.17 GeV is the weighted average of the two σ parameters from the parametrization. If one subtracts $\Gamma_Z = 2.5$ GeV from 3.17 GeV one obtains 1.95 GeV, which is not so far from the value $\sigma_M = 1.39$ GeV. This check is very crude, and a more careful verification of the mass resolution will be attempted in the future.

5.2 Finding the Minimum

The shape of ΔF is not simple due to the finite numbers of events in each region, and in fact there tend to be many local minima. This gave us some difficulty – a naive calculation of ΔF displayed jumps. In principle this was OK since the jumps and difference in local minima corresponded to a fraction of σ_a, but we did not like the idea of a chaotic result.

After some investigations and a little trial-and-error, we settled on the following prescription.

1. find an approximate local minimum $\Delta F_{\rm min}$.
2. sample ΔF in several points around this minimum correspond to $\Delta F < \Delta F_{\rm min} + 1$.
3. fit these points to a parabola as a function of a.
4. define ΔF with respect to this parabola at $a = 0$.
5. use the parabola to find $a_{\rm BEST}$ and σ_a as well.

This procedure produced no biases and lead to an intuitive and clean behavior of ΔF as a function of x. We checked that there were no strange differences between the answer obtained this way and that obtained by brute-force searching for the minimum. If a true signal were present, then one could discuss possible tiny differences in the significance of the peak. For setting limits, the difference is a fraction of σ_a and hence, irrelevant.

Fig. 8 shows four examples of the true chaotic ΔF, the parabola, and the bounds on the amplitude.

5.3 The 4–9 Region

We carried out the scan for this region using Eq. (1), the continuum parametrization given in Sec. 4 and a Gaussian for the signal with a width given by Eq. (5). The number of events is listed in Table 1.

The best fitted amplitude, $a_{\rm BEST}$, oscillates around zero as we step across the mass range. The change in the negative log-likelihood, ΔF, shows only modest spikes toward negative values, and many of these correspond to $a_{\rm BEST} < 0$. See Fig. 9 for the actual results. In short, there is no signs of any signal.

We discuss the particular case of $M_{\mu\mu} = 7.25$ GeV later, in Sec. 7.

5.4 The Υ Region

Although this area has been extremely well studied, especially in e^+e^- collisions, it is still tempting to look here for anomalies, as there is a fair amount of space available for small peaks. Consequently, we have scanned this area as we have scanned the others. Fig. 10 shows the ΔF and $a_{\rm BEST}$ results as a function of mass. Although there is a tiny peak near $M_{\mu\mu} = 9.2$ GeV, it is not significant.

5.5 The 13–84 Region

We scanned the region between the Υ resonances and the Z-peak. See Fig. 11 shows ΔF and $a_{\rm BEST}$ as a function of mass. There is no evidence for any new peaks in this region.

5.6 The Z-peak Region

We scanned the region around the Z-peak. This may seem odd, looking for a peak on top of a peak, but there is a possibility of observing something like $A \to \mu^+\mu^-$ which would be narrower than the Z-peak, and much smaller, obviously. The results of the scan are shown in Fig. 12. It is clearly more difficult to identify a peak in this region since there is a larger number of events from the Z-peak which can fluctuate up or down. This is reflected in the gentle maximum in the dashed line in the lower plot indicating that the uncertainty σ_a is

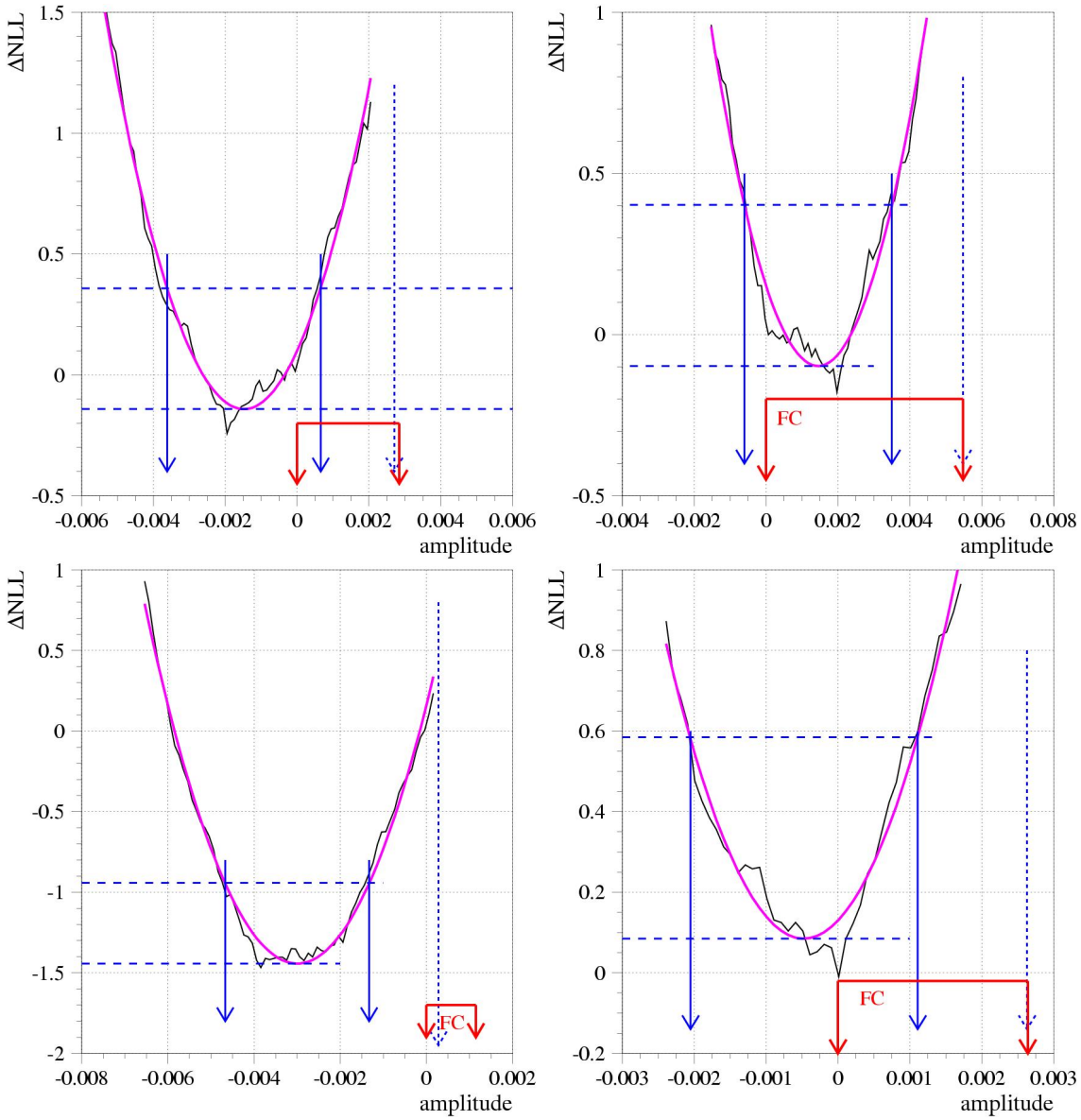

Figure 8: *four example scans, from real data. The chaotic nature of the raw* ΔF *is evident. The parabolas are used for defining* ΔF *as used in the scans, as well as* $a_{\rm BEST}$ *and* σ_a*. The thick red line shows the range allowed at* 95% *CL by the Feldman-Cousins prescription.*

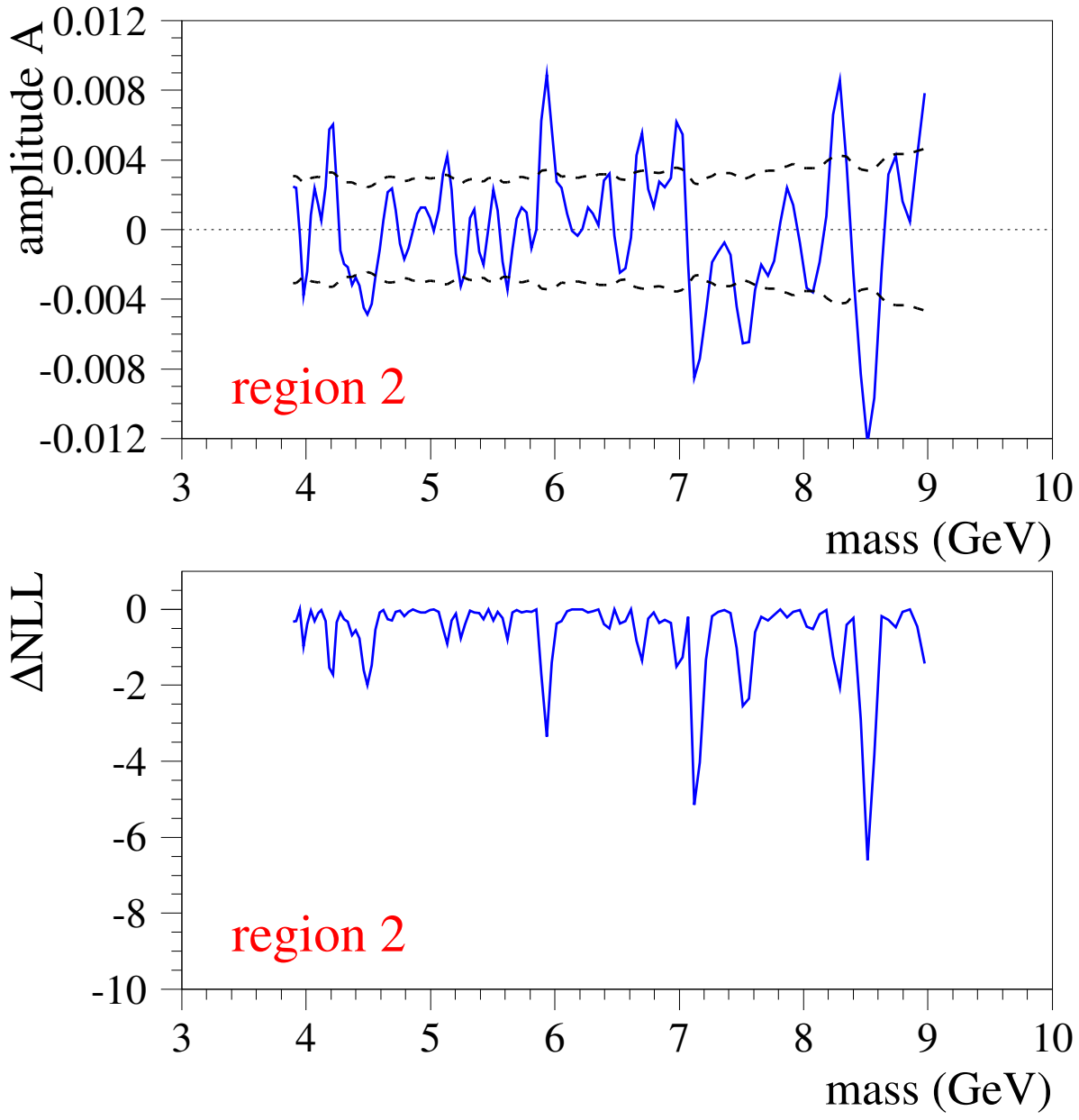

Figure 9: *scan of region 2. Top:* ΔF *as a function of mass. Bottom:* a_{BEST} *as a function of mass. The dashed lines show the expected* σ_a *in the absence of signal.*

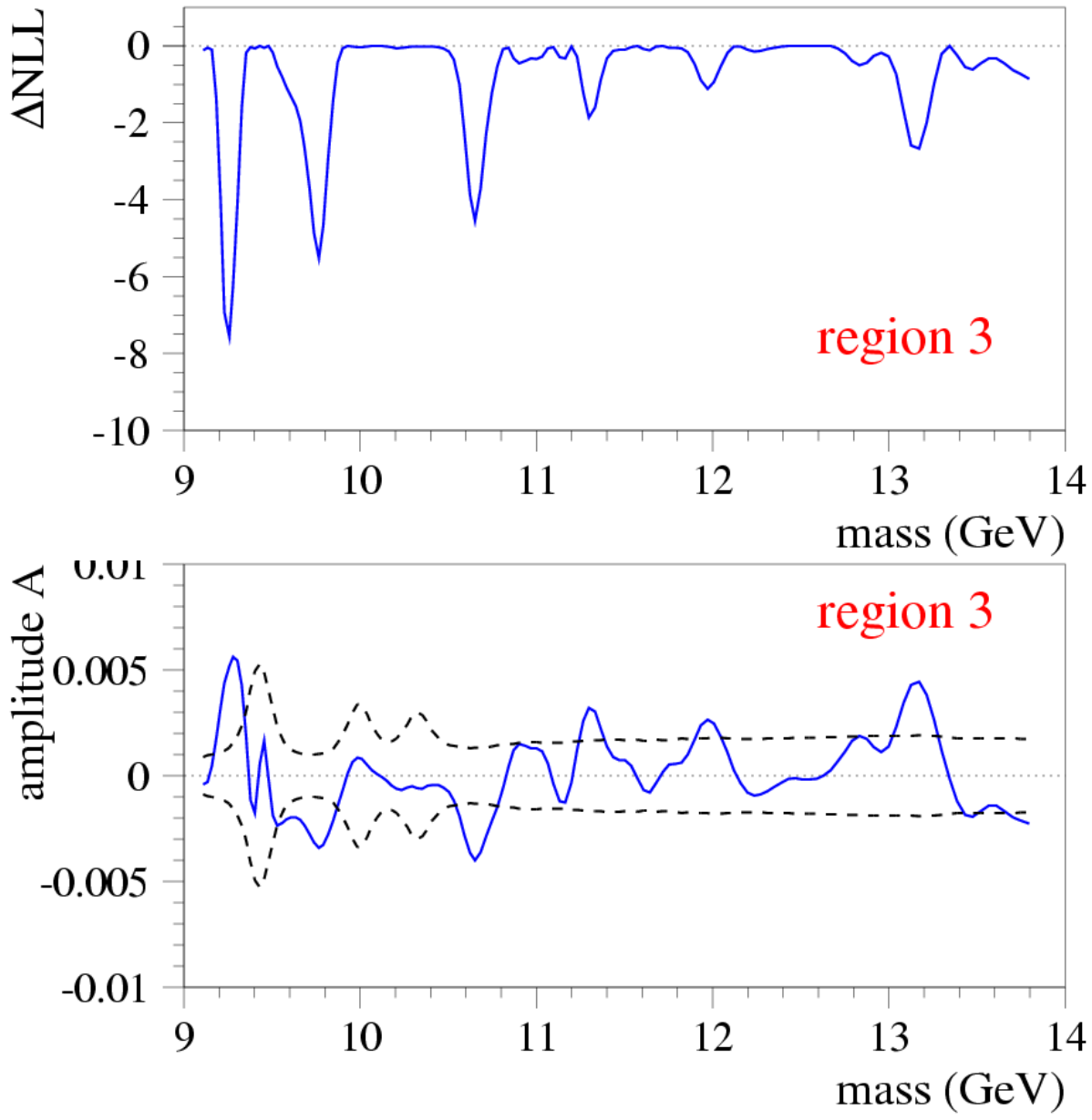

Figure 10: *scan of region 3. Top: ΔF as a function of mass. Bottom: a_{BEST} as a function of mass. The dashed lines show the expected σ_a in the absence of signal.*

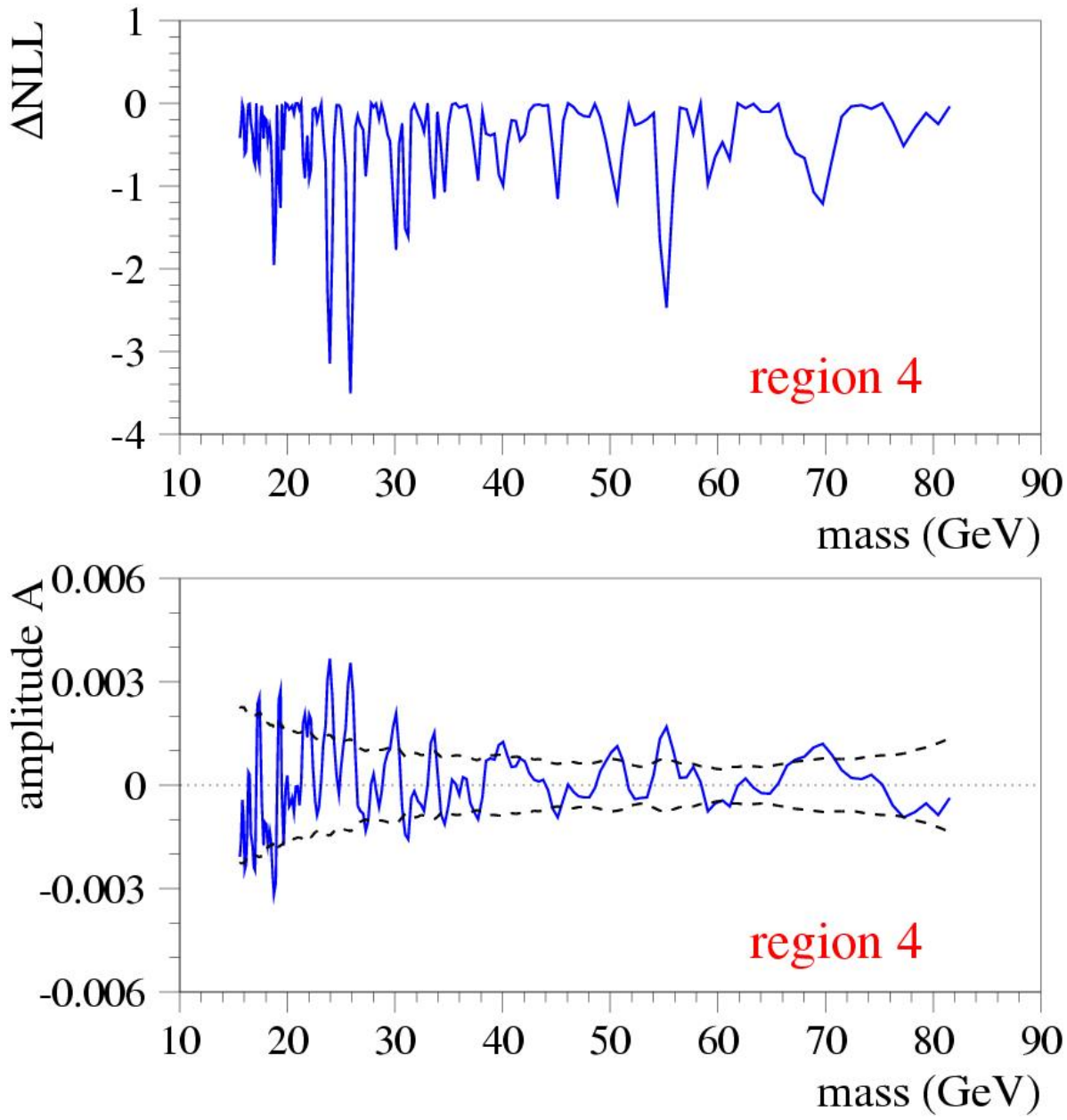

Figure 11: *scan of region 4. Top: ΔF as a function of mass. Bottom: a_{BEST} as a function of mass. The dashed lines show the expected σ_a in the absence of signal.*

larger on the Z-peak. There is a slight excess around $M_{\mu\mu} = 91$ GeV which is is not evident in Fig. 5. It significance is slightly more than "2σ" and so is far from significant.

5.7 The High-Mass Region

We scanned the high-mass region, up to 200 GeV only. The result is shown in Fig. 13, which indicates no evidence for any signal.

6 Limits

None of the regions 2–6 show any signs for a new resonance, so we turn to setting limits on signal cross sections. First we review the basis and our implementation of the Feldman-Cousins prescription. This allows us to obtain an upper limit on the number of signal events. In order to convert this into a cross section, we need to understand something about the muon efficiency, the acceptance, and the luminosity.

6.1 The Feldman-Cousins Prescription

The Feldman-Cousins prescription [3] was designed to solve two problems:

- the preferred value for a parameter may fall inside an unphysical region.
- the distinction between setting a limit on a signal and quoting evidence, discovery or making a measurement is arbitrary and historical. This leads to under-coverage.

We refer to reader to the original article for a thorough discussion – we recap only a few points here.

One starts by constructing "confidence belts" for an observable a in terms of the physical parameter μ one wants to extract from the data. (In the original article, X represents the observed / measured quantity. We use a here since that is our measured quantity, and we have been using x for the mass.) The authors consider two examples: a Poisson distribution and a Gaussian. Our amplitude, a, is distributed as a Gaussian, so that is the case that pertains here. The physical parameter μ is the number of signal events; naively one thinks of $\mu = a \times N_{\rm tot}$ within a given region.

We reproduced the results of the Feldman-Cousins paper, for a 95% CL – see Fig. 14. Given an actual, observed value for X (in the figure), one infers range of μ given by the two lines. For example, if $X = 2$ (corresponding in our case to $a_{\rm BEST} = 2\sigma_a$), then $0.4 < \mu < 4$ at 95%CL. From the shape of the contours it is clear that the lower bound for μ is never negative, by construction. Note, also, that for a mild fluctuation (such as $a_{\rm BEST} = 2\sigma_a$), $\mu = 0$ does not lie in the 95% confidence belt.

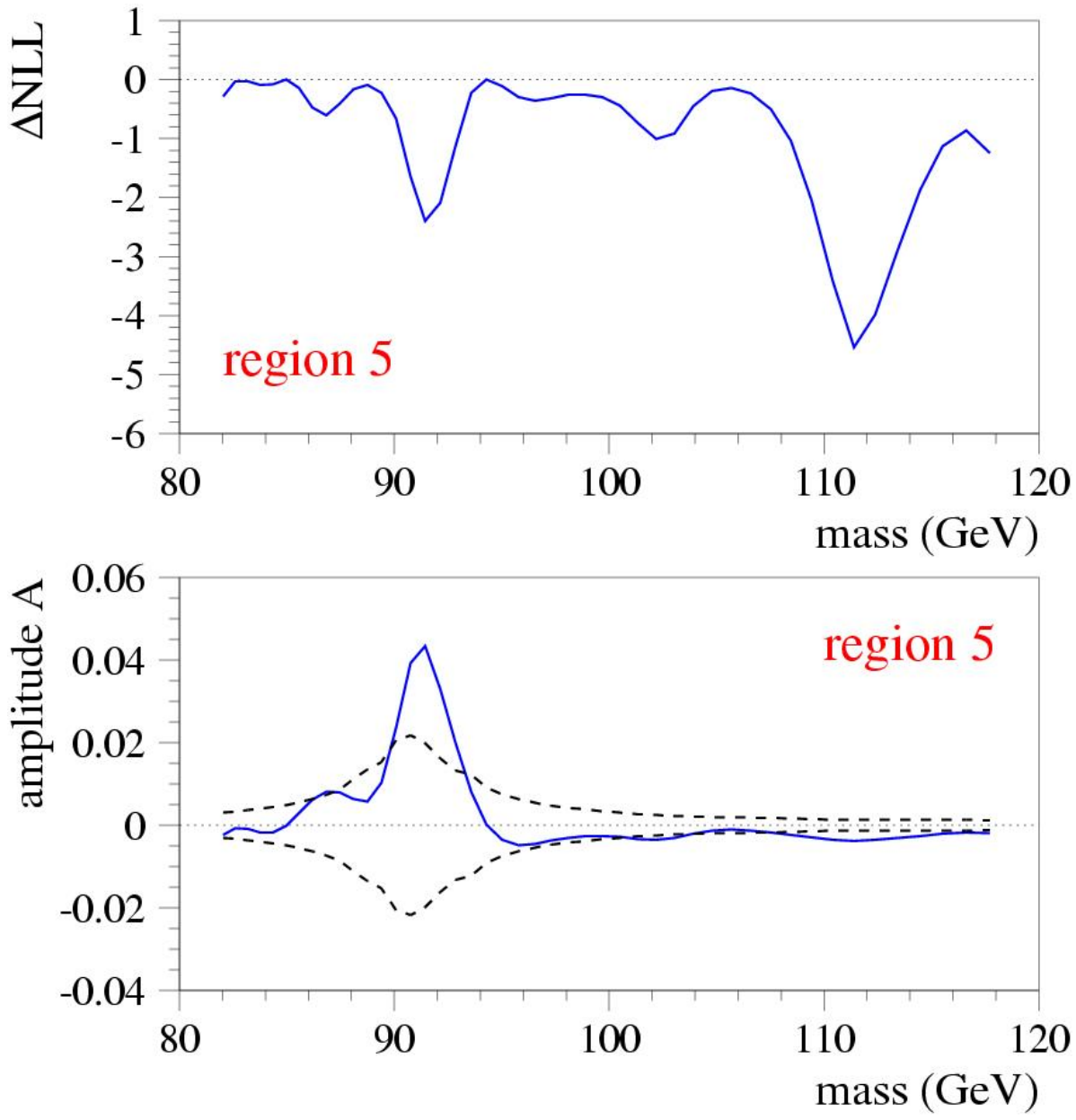

Figure 12: *scan of region 5. Top: ΔF as a function of mass. Bottom: a_{BEST} as a function of mass. The dashed lines show the expected σ_a in the absence of signal.*

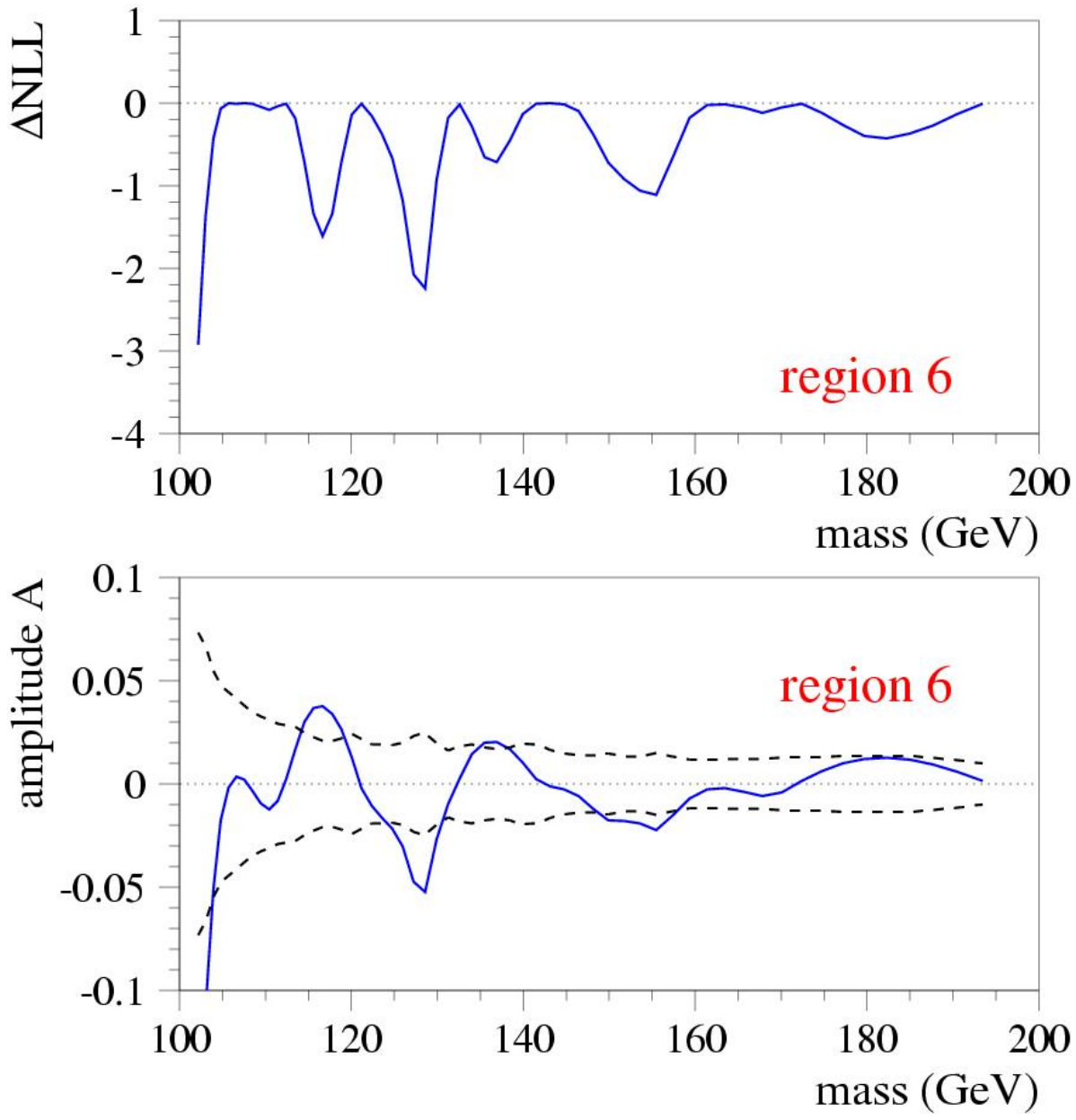

Figure 13: *scan of region 6. Top: ΔF as a function of mass. Bottom: a_{BEST} as a function of mass. The dashed lines show the expected σ_a in the absence of signal.*

We computed the coordinates of this belt over a wider range than in the Feldman-Cousins article, and wrote a routine which interpolates between points to obtain the range for μ for any X.

We checked that our implementation of the the Feldman-Cousins procedure led to correct results when the fitted amplitude was zero, or significantly greater than zero. For several interesting examples from the actual analysis, see Fig. 8.

6.2 Efficiency, Acceptance and Luminosity

We will use the yield at the Z-peak and the known cross-section for $p\overline{p} \to Z \to \mu^+\mu^-$ to set the overall value for $\epsilon \times A \times \mathcal{L}$, where ϵ is the net muon efficiency, A is the acceptance (as a function of mass), and $\mathcal{L}$ is the total luminosity, which we know to be approximately 195 pb^{-1}.

6.2.1 Normalization

In the mass range $66 < M_{\mu\mu} < 116$ GeV, we observe 3843 events passing our cuts. Our rough estimates for the identification efficiency is 0.8, for the isolation requirement, 0.9, for muon reconstruction, 0.95, and for the trigger, 0.80 per event. The overall acceptance times efficiency is $A \times \epsilon = 0.077$. Ignoring backgrounds, which we know to be very small in this mass range [7], and taking the cross section to be $\sigma = 255$ pb [4], we predict 3824 events. We conclude that $A \times \epsilon \times \mathcal{L} = 15.0$ pb^{-1}. We use that figure for normalizing all of the cross sections:

$$\sigma(x) = \frac{N_{\rm ev}}{\left(\frac{A(x)}{A(M_Z)}\right) \times 15.0 \text{ pb}^{-1}}.$$

In this we assume no variation of ϵ with mass. We discuss the systematic uncertainty associated with the assumption below.

6.2.2 Acceptance vs. Mass

The acceptance varies with mass. We have estimated the acceptance function $A(x)$ by running a generator-level Monte Carlo simulation and applying the basic cuts $p_T > 5$ GeV and $|\eta| < 1$ for both muons. We fit the function $A(x)$ as a function mass in several piecewise continuous functions which are forced to agree at their mutual boundaries. The result is displayed in Fig. 15. We plan to replace this with an acceptance function which is based on the full simulation.

For $M_{\mu\mu} > 12$ GeV, this works well. Below that point, the requirement $p_T > 5$ GeV suppresses events which small q_T, and the fidelity of the simulation becomes an issue. Furthermore, the acceptance will depend on the assumed q_T distribution, which is different for Drell-Yan and for, say, $\Upsilon(1s)$ events. We discuss this model-dependence in detail below.

First we check that our parametrized acceptance curve (Fig. 15) successfully represents the distribution obtained at generator level. Fig. 16 shows a direct comparison of the

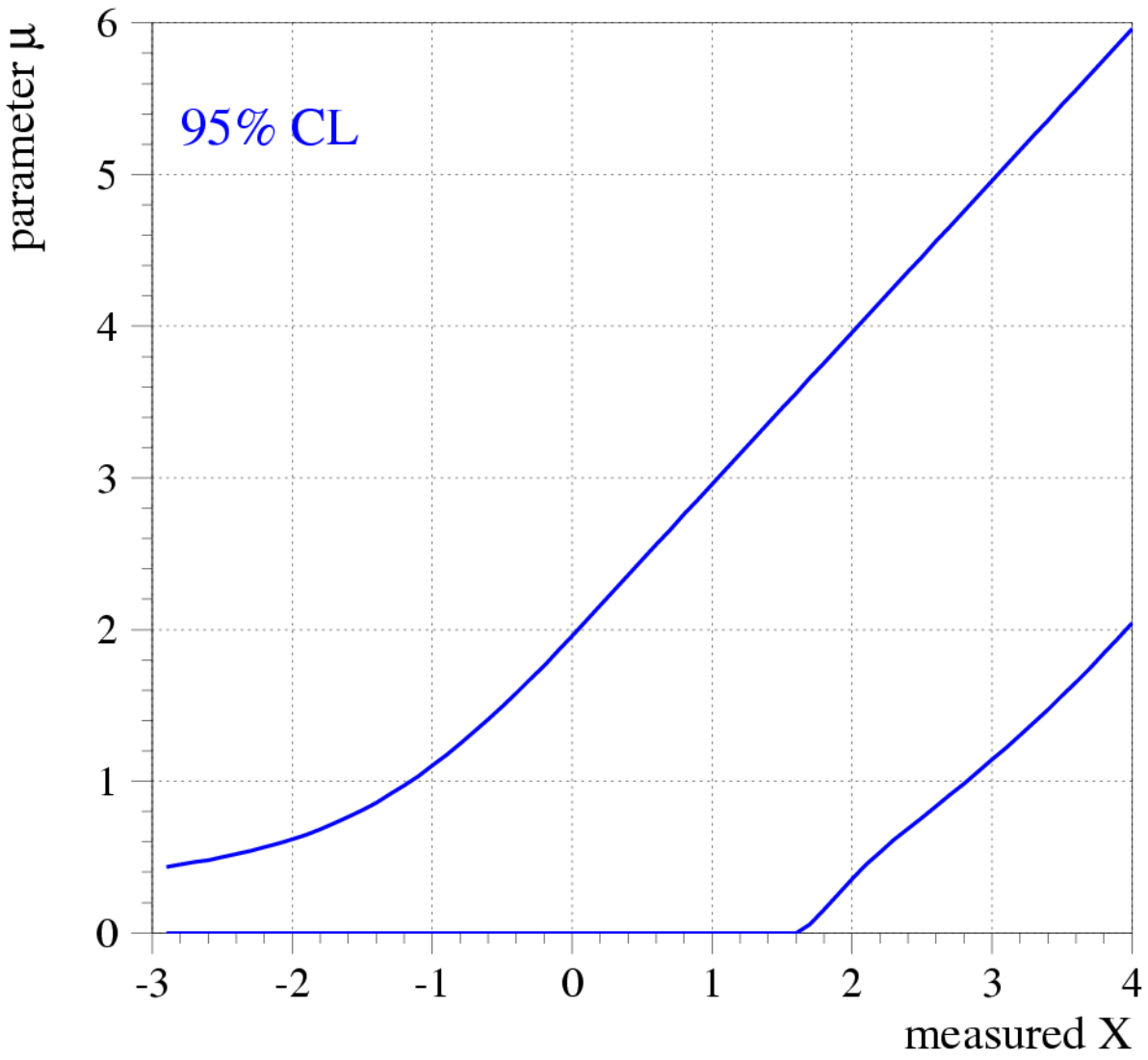

Figure 14: *Feldman-Cousins confidence belt for a parameter μ which must be non-negative, and a Gaussian-distributed observable, X. This belt corresponds to 95% CL.*

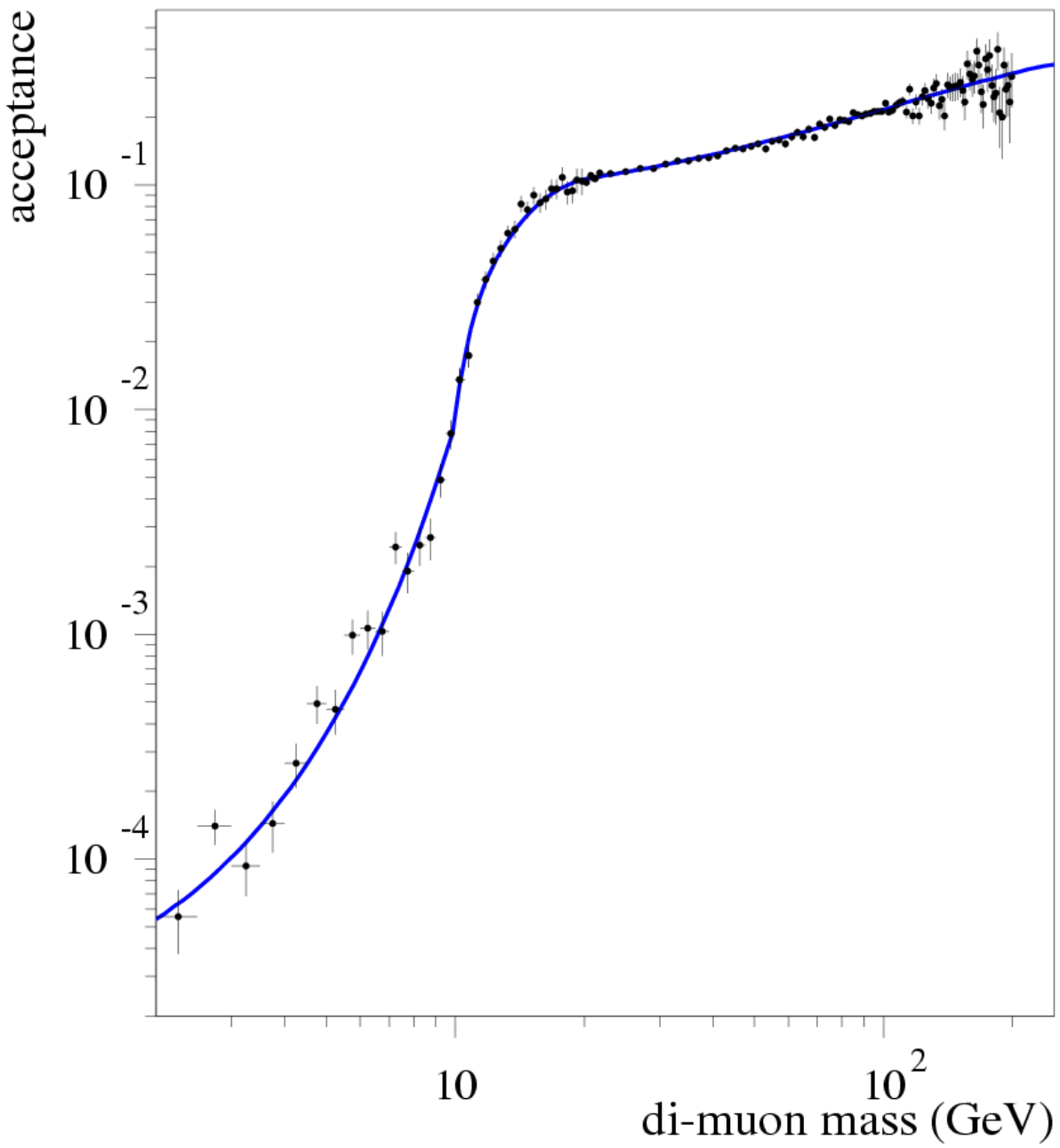

Figure 15: *acceptance as a function of mass. The solid blue line is a parametrization.*

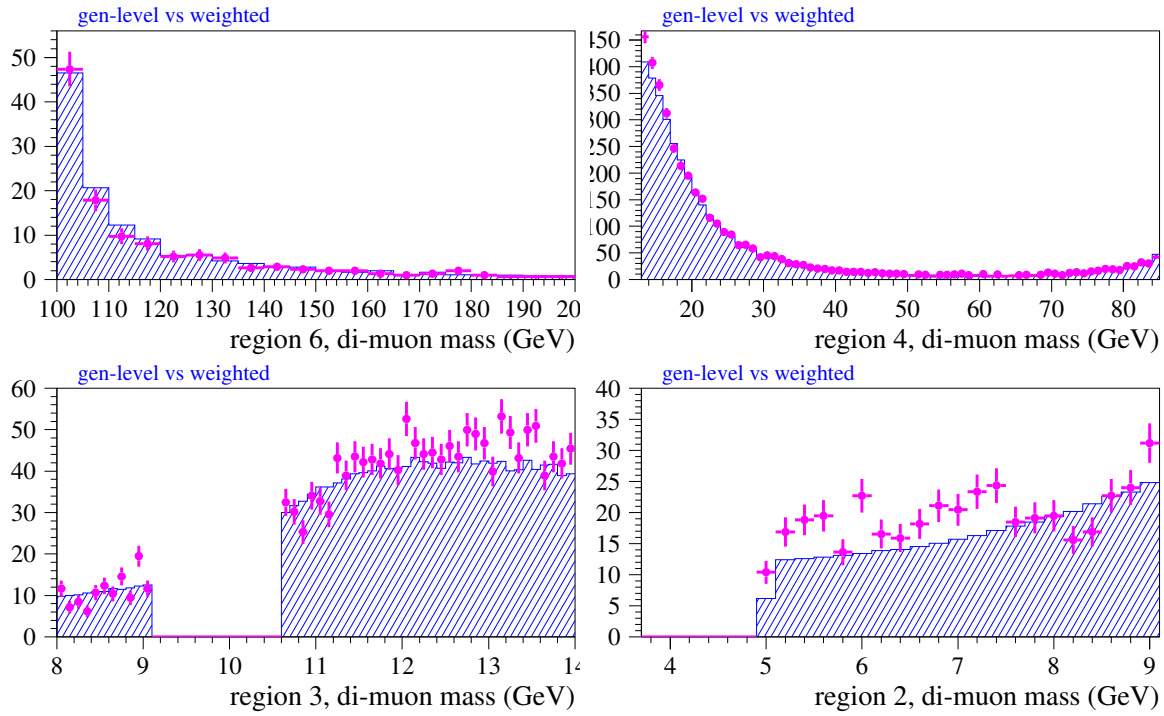

Figure 16: *generator-level comparison of accepted events (points) and the generated mass spectrum weighted by the acceptance function (shaded histogram).*

generator-level mass distributions for four regions. The points represent the events which pass the nominal acceptance cuts $p_T > 5$ GeV and $|\eta| < 1$ (both muons), and the shaded histogram is the generated mass distribution weighted by the acceptance function displayed in Fig. 15. The agreement is good, except that the acceptance function may be a little bit too low for $M_{\mu\mu} < 7.5$ GeV. We do not attempt to correct this deficiency.

Next we compare the fast simulation with nominal acceptance cuts to the full simulation – see Fig. 17. The full simulation is Drell-Yan set `z8v2gt` generated by John Zhou with a minimum di-muon mass of 5 GeV. In all of the comparisons we show in this section, we therefore impose $M_{\mu\mu} > 5$ GeV. As seen in Fig. 17, the agreement between the fast and the full simulation is very good, so we can rely on the acceptance estimate that we obtained for Drell-Yan events from the fast simulation.

6.2.3 Full Simulation vs. Real Data

The ultimate test of our understanding of the acceptance is the direct comparison of the mass distribution to data. For this, we must understand contributions from non-Drell-Yan sources.

Based on studies by the New Mexico group [5], we expect that the main non–Drell-Yan

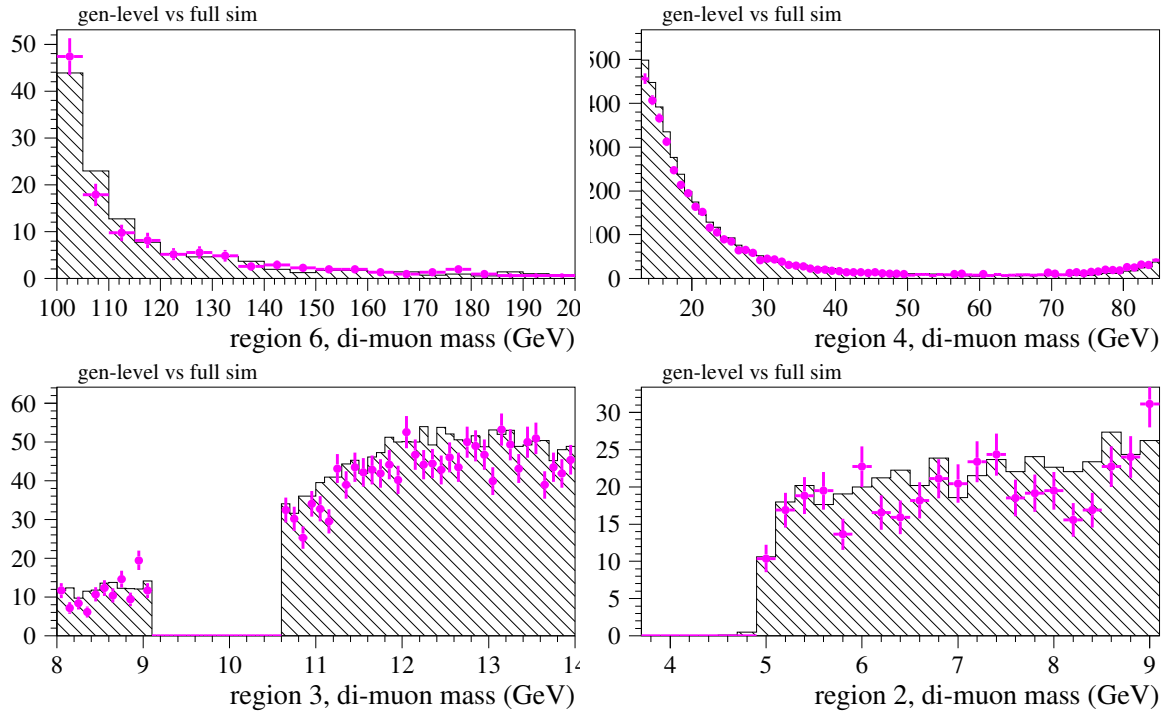

Figure 17: *comparison of accepted generator-level events (points) and the full simulation (shaded histogram).*

contribution will come from heavy-flavor production. We will use the same-sign events to help estimate this contribution. Considering the origin of muons in $b\bar{b}$ events, one expects that most of them will have opposite-sign, so one must be prepared to scale up the contribution inferred from the same-sign sample. For the analysis done by the New Mexico group, for example, the ratio of opposite-sign to same-sign samples is about three.

In order to get a handle on this scale factor, we generated a very large sample of $b\bar{b}$ events using PYTHIA, and applied our nominal kinematic and fiducial cuts to any muons produced. The fraction of such events was very small; nonetheless, we are able to see that the opposite-sign contribution is indeed larger than the same-sign by a factor of 1.5 ± 0.4.

We do not use this number since it is based on a generic PYTHIA simulation at generator-level. Rather, we use certain kinematic distributions to tune to Drell-Yan template from the full simulation and the same-sign distribution from data to describe the opposite-sign distribution from the data (which is the basis for our search). In particular, we look at the distributions of the p_T of the two muons (two entries per event), of the di-muon transverse momentum (q_T), and the rapidity distribution y of the di-muon pair, in addition to the mass ($M_{\mu\mu}$) distribution itself. Region-by-region, these are able to distinguish Drell-Yan and same-sign (*i.e.,* heavy-flavor) contributions.

First, we scale the simulated Drell-Yan distributions to match the observed number of events at the Z-peak (region 5). There are no same-sign events in this region, nor is there any contribution from $\tau^+\tau^-$ pairs. If the acceptance from the simulation were correct, and if there were no heavy-flavor contributions, then the mass distributions should be reproduced region-by-region, without further modifications.

The comparison of the Drell-Yan simulation and the real data for region 5 (the Z-peak region) is shown in Fig. 18. The agreement is quite good, as expected. Next we show region 6 (the "high-mass" region) in Fig. 19, where again there is no contribution from heavy-flavor or $\tau^+\tau^-$.

In region 4, which falls below the Z-peak and above the Υ resonances, we begin to see the appearance of the heavy-flavor contribution for $M_{\mu\mu} < 22$ GeV. This is also seen by the New Mexico group [5]. In Fig. 20 we compare the sum on the simulation and same-sign to the opposite-sign from the data. In this figure, the points represent the opposite-sign data, the green histogram represented the simulated Drell-Yan contribution scaled according to the yield at the Z-peak, and the red histogram presents the same-sign spectrum scaled so that the sum of the total number of same-sign events and the simulated Drell-Yan events matches the number of opposite-sign events, for this mass region. The yellow histogram represents the sum of the scaled same-sign and the simulated Drell-Yan contributions, and is directly comparable to the points. Note that these histograms are *not stacked*. The agreement is very good for all four distributions. We tried, as a counter-example, to fix the same-sign with no scale factor, and scale up the Drell-Yan spectrum. This produced distributions which were much too hard in q_T and p_T, and made a noticeably poorer match to the mass distribution. Thus, we believe that our acceptance in this region is correctly given by the simulation, and the scale factor for the same-sign distribution is 2.05 with a small statistical uncertainty.

Next we consider region 3, the Υ region. Since Υ production was not included in the simulations, we cut out a mass window $9.1 < M_{\mu\mu} < 10.6$ GeV. Fig. 21 compares the prediction to the data; the colors of the plots, etc., are the same as in Fig. 20. Once again, the best match to the opposite-sign data is obtained by scaling up the same-sign spectrum, this time by a factor of 2.03. We do not scale-up the simulated Drell-Yan spectrum at all. There is some evidence, however, for a shortfall for $8 < M_{\mu\mu} < 9.1$ GeV; this might indicate that the acceptance is underestimated in that region. We do no attempt any correction.

Finally, we show the comparisons for region 2 in Fig. 22. As in regions 3&4, the sum of the numbers of simulated Drell-Yan and the same-sign data is smaller than the number of opposite-sign events. However, if we scale up the same-sign events, we obtain spectra for p_T and q_T which are too soft. We also obtain a rapidity distribution which is a bit too pointy. Instead, a very good description is obtained if we scale up the Drell-Yan contribution by a factor of 2, and the same-sign by a factor of 1.55, as displayed in Fig. 22. It may be that this mix of scale factors also would apply to the interval $8 < M_{\mu\mu} < 9.1$ GeV in region 3. Although there is a possibility, therefore, that the acceptance for Drell-Yan events for $M_{\mu\mu} < 9$ GeV is significantly underestimated, we do not try to correct our acceptance (cf. Fig. 15) in this region. Given that we will set cross-section limits as a function of mass, this is a conservative choice. We feel that more work would be needed to justify such a correction, and this work has not been done.

In summary, the agreement between the predictions based on the fully simulated Drell-Yan events and rescaled same-sign spectra from real data, and the opposite-sign data which we use for our search, is quite good even in regions where the acceptance is falling rapidly.

6.2.4 The Υ Yield

The $\Upsilon(1s)$ provides another benchmark for testing our understanding of the acceptance. It is a non-trivial one, since already at $M_{\mu\mu} = 9.34$ GeV the acceptance is falling rapidly and only the high-q_T events survive the momentum requirements. Furthermore, PYTHIA does not predict correctly the q_T spectrum for the $\Upsilon(1s)$ (see Fig. 24, and we will have to employ the measurement done by CDF in Run I [8] and also the one done by DØ in Run II [9].

The first step is to obtain the acceptance as a function of q_T. This is obtained from PYTHIA and is displayed in Fig. 23 along with a simple parametrization. If we convolve this acceptance with the PYTHIA q_T distribution, we obtain the same number as simply counting the number of accepted events, as we should. If we convolve this acceptance with the differential cross-section measured by CDF, we obtain $A_\Upsilon = 0.0123$, which is about a factor of two higher. Given the acceptance of the Z (which is 0.206), the numbers of Z and $\Upsilon(1s)$ events, and the Z cross-section, we can obtain a cross-section $\sigma(\Upsilon(1s))$ as follows:

$$\sigma(\Upsilon(1s)) = \left(\frac{3134}{3871}\right) \times \left(\frac{0.0123}{0.206}\right) \times 255 \text{ pb} = 3540 \pm 85 \text{ pb}$$

where the error is purely statistical coming from the number of events; the uncertainty on the cross-section normalization amounts to about 2.8%, or ±98 pb. The CDF measurement

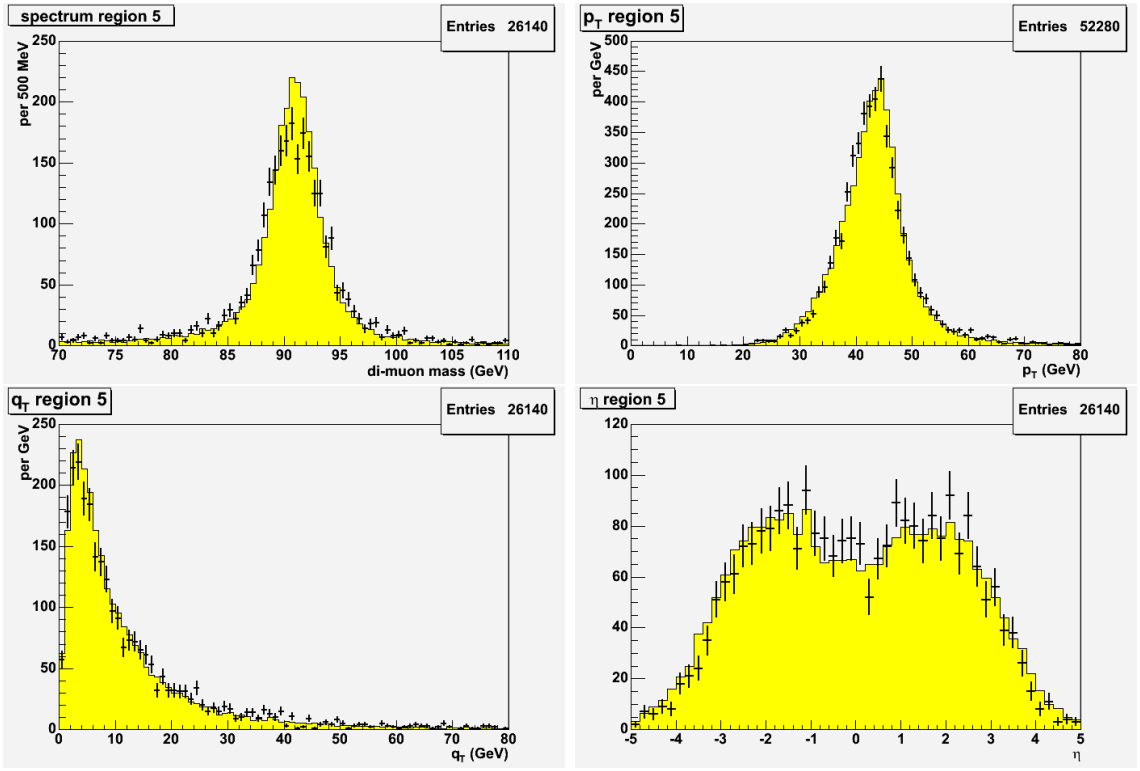

Figure 18: *comparison of opposite-sign events from data (points) to the full simulation (yellow histogram), for events in region 5 (the Z-peak region).*

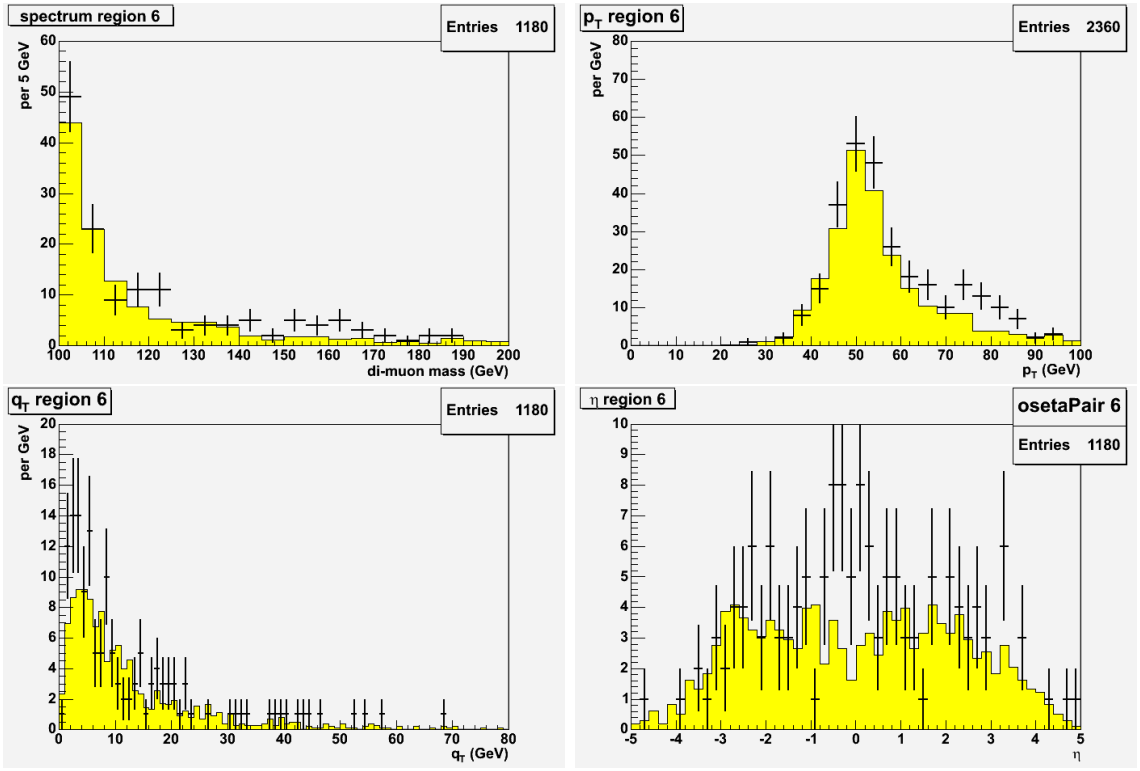

Figure 19: *comparison of opposite-sign events from data (points) to the full simulation (yellow histogram), for events in region 6 (the high-mass region).*

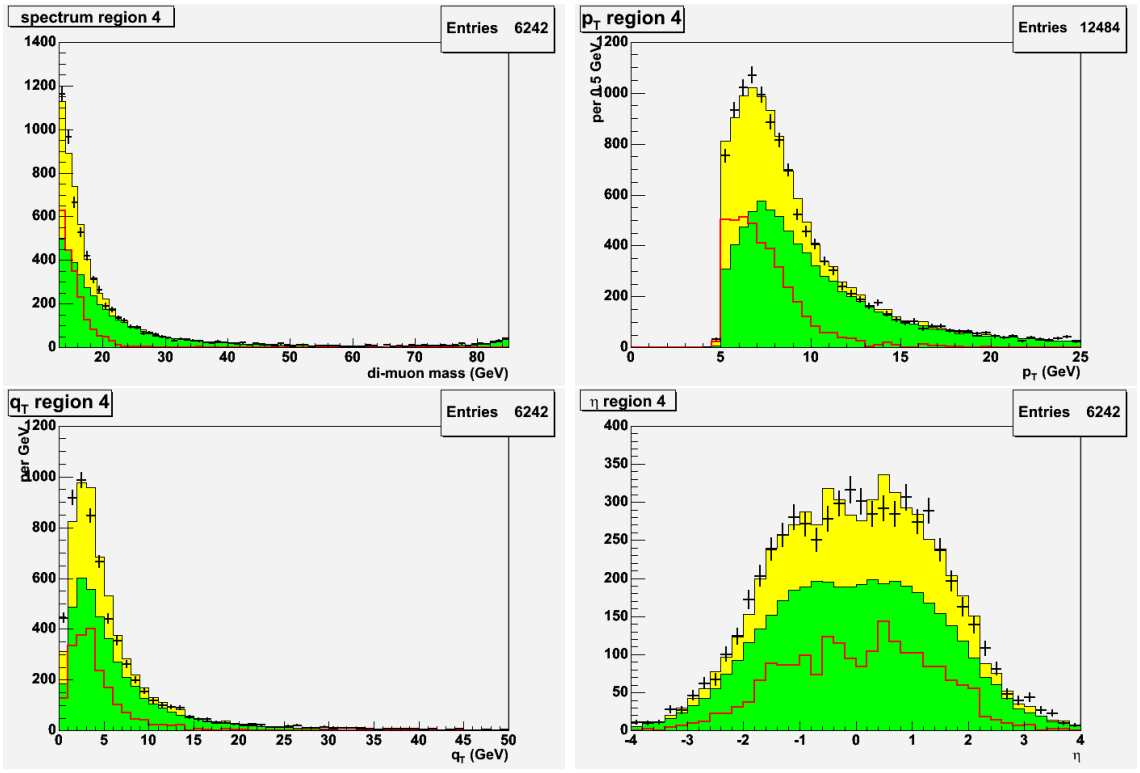

Figure 20: *comparison of opposite-sign events from data (points) to the prediction (yellow histogram), which is the sum of the simulated Drell-Yan events (green histogram) and the scaled same-sign spectrum from data (red histogram), for events in region 4 (the "11 – 84" region).*

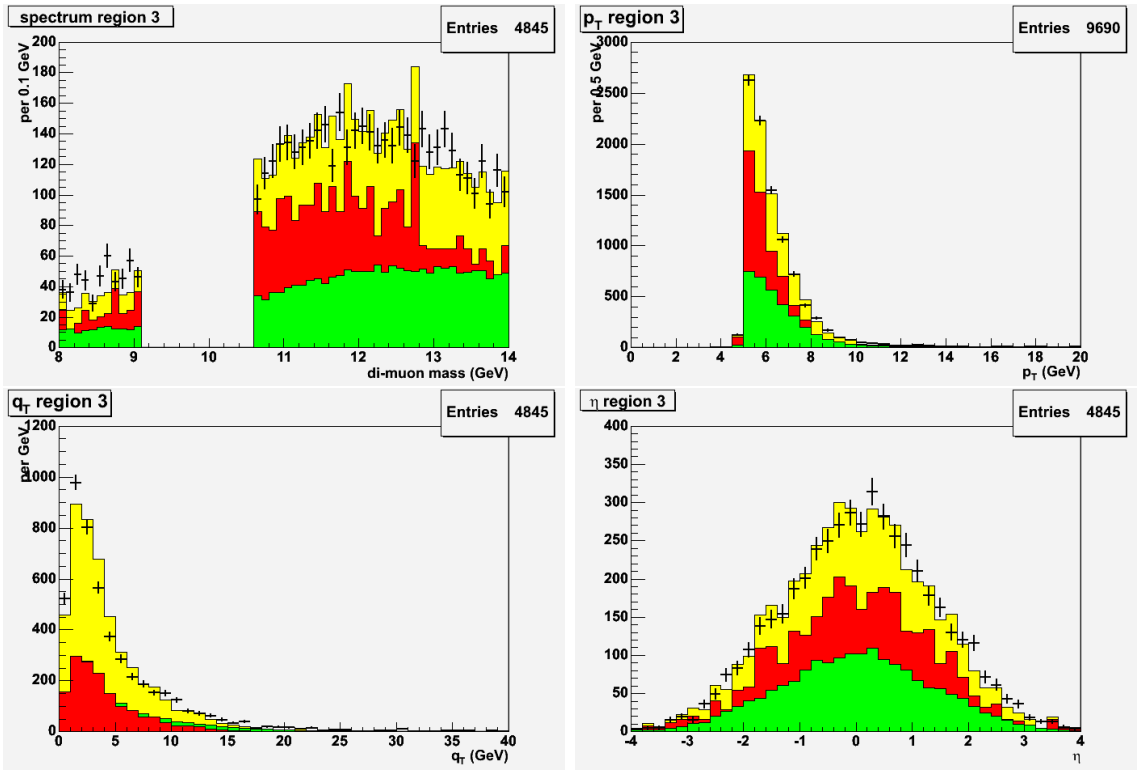

Figure 21: *comparison of opposite-sign events from data (points) to the prediction (yellow histogram), which is the sum of the simulated Drell-Yan events (green histogram) and the scaled same-sign spectrum from data (red histogram), for events in region 3 (the* Υ *region).*

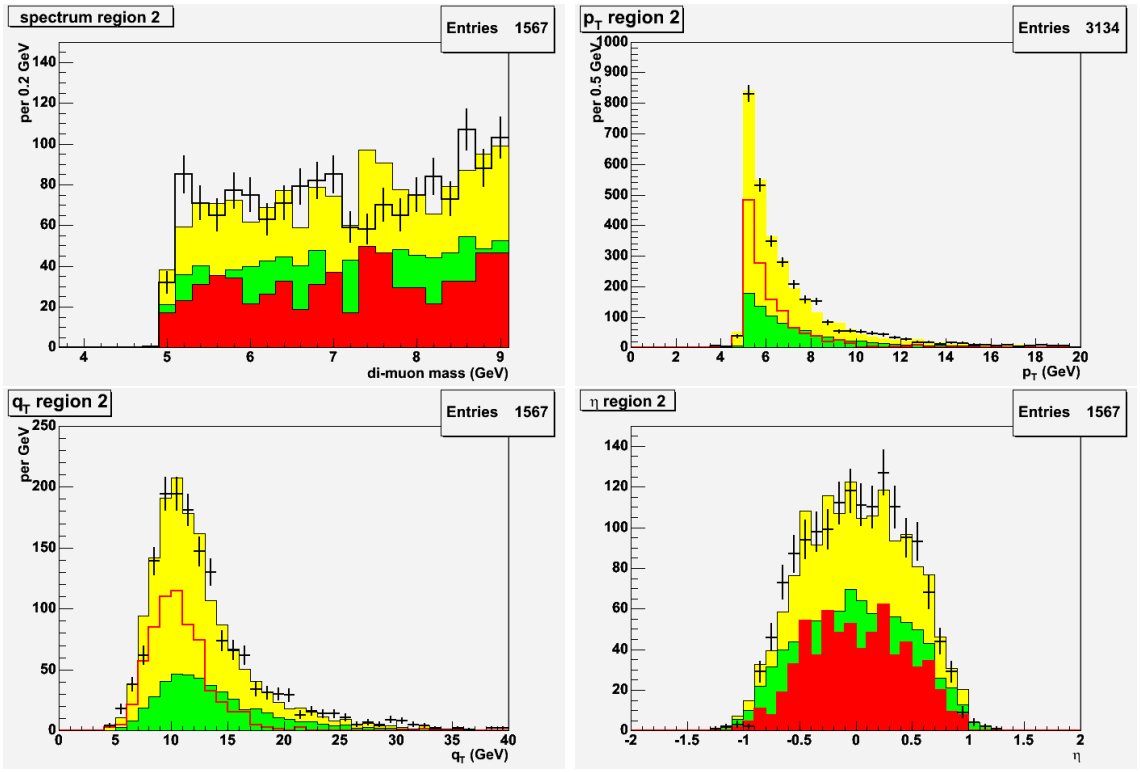

Figure 22: *comparison of opposite-sign events from data (points) to the prediction (yellow histogram), which is the sum of the simulated Drell-Yan events (green histogram) and the scaled same-sign spectrum from data (red histogram), for events in region 2 (the "4–9" region).*

gives

$$\frac{d\sigma}{dy} = 670 \pm 15 \pm 18 \text{ pb}$$

which applies for $y_{\mu\mu}$ near zero. The DØ measurement is $d\sigma/dy = 732 \pm 19 \pm 73 \pm 48$ pb, where the last uncertainty pertains to the luminosity. In order to obtain a total cross-section, we integrate the rapidity distribution from PYTHIA, which is displayed in Fig. 25, normalized according to the CDF measurement. Integrating over all rapidity, we obtain $\sigma = 3366 \pm 118$ pb, where the error is simply scaled from the CDF measurement and does not include the probably small increase expected for the higher center-of-mass energy, nor any systematic uncertainty due to the use of the PYTHIA rapidity distribution. The difference in cross-section is

$$\sigma_{\text{inferred}} - \sigma_{\text{CDF I}} = 174 \pm 176 \text{ pb},$$

which shows adequate agreement. If one wanted to demand better agreement, one would guess that the acceptance were, once again, slightly underestimated. A more likely explanation is that the cross-section for $\sqrt{s} = 1.96$ TeV should be a little higher than the CDF Run I measurement. If we use the central value from the DØ measurements, for example, then the difference in cross-section would be $\Delta\sigma = -137$ pb.

The conclusion is that we understand the acceptance for $\Upsilon(1s)$ at least at the 10% level, or better, provided that the rapdity distribution from PYTHIA (Fig. 25) is not too far off from reality. The acceptance for $\Upsilon(1s) \to \mu^+\mu^-$ in this analysis is good for $|y| < 0.9$.

It is worth pointing out that the DØ analysis demonstrates with small uncertainties that the shape of the differential cross-section $d\sigma/dq_T$ hardly changes across the rapidity range $-1.8 < y < 1.8$. Also, the shape of the cross-section $d\sigma/dq_T$ shows no change between $\sqrt{s} = 1.8$ TeV and 1.96 TeV – see Fig. 26.

6.2.5 Acceptance vs. q_T for Υ-like Objects

It turns out that the acceptance for $\Upsilon(1s)$ is about twice that for Drell-Yan events of the same mass, due mainly to the more central production of the Υ mesons. We need to make a separate estimate for the acceptance of Υ-like objects as a function of mass, in order to interpret the results in the low-mass region 2.

We generated a series of Υ-clones with masses of 4, 5, 6, 7, 7.25, 8 and 9 GeV, and obtained for each one an acceptance function similar to the one displayed in Fig. 23. We parametrized each one in the same manner: a straight line with a flat top. The intercepts, slopes and flat-top values evolved with mass just as one would expect – the bias in q_T gets worse as the mass falls.

In order to obtain a net acceptance, we need to have a model for the differential cross-section $d\sigma/dq_T$, since PYTHIA is unreliable for this. Clearly $d\sigma/dq_T$ will soften as the mass decreases. Hence, so will the mean q_T. We computed $\langle q_T \rangle$ for each of our Υ-clones, and found that it decreases linearly with mass; according to PYTHIA, we have

$$\langle q_T \rangle = 3.42 \text{ GeV} + 0.213\,(M_{\mu\mu} - 9.34 \text{ GeV}) \tag{8}$$

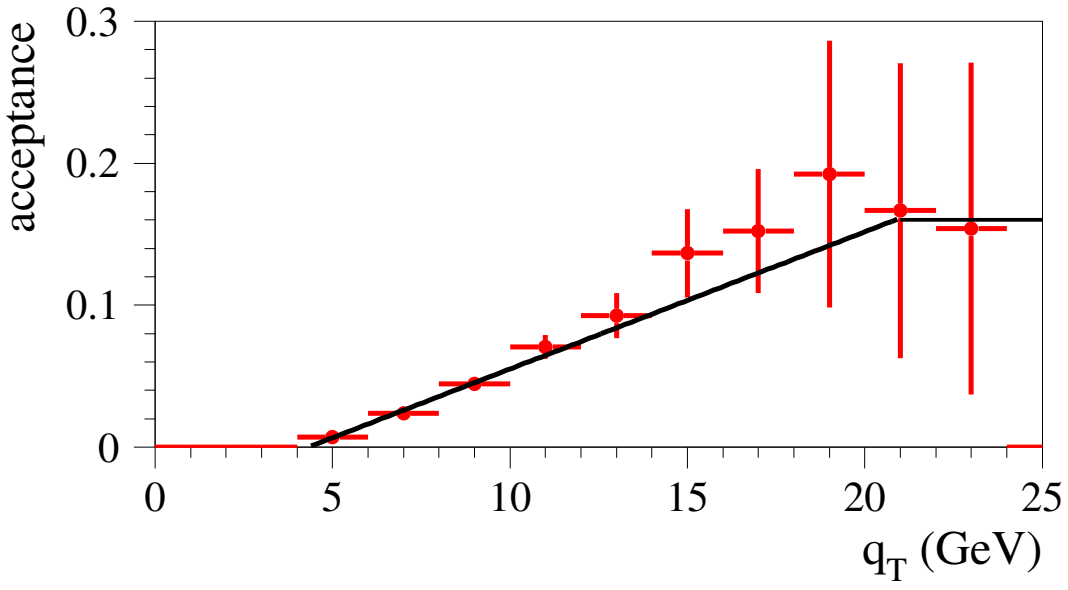

Figure 23: *acceptance as a function of q_T obtained from PYTHIA. The lines show a simple parametrization used when computing the net acceptance.*

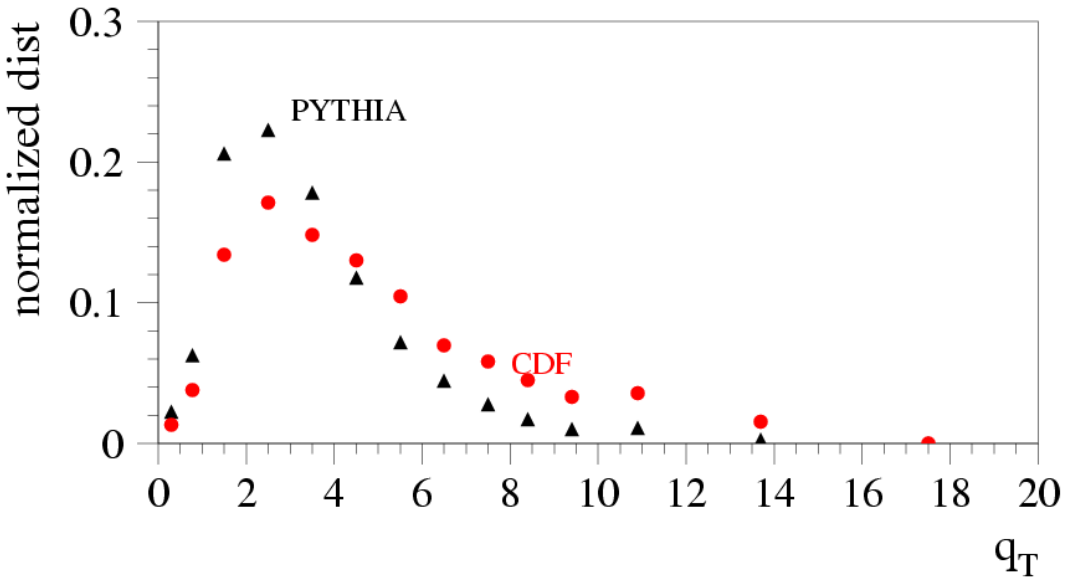

Figure 24: *q_T distributions from straight PYTHIA (triangles) and the CDF Run I measurement (circles)*

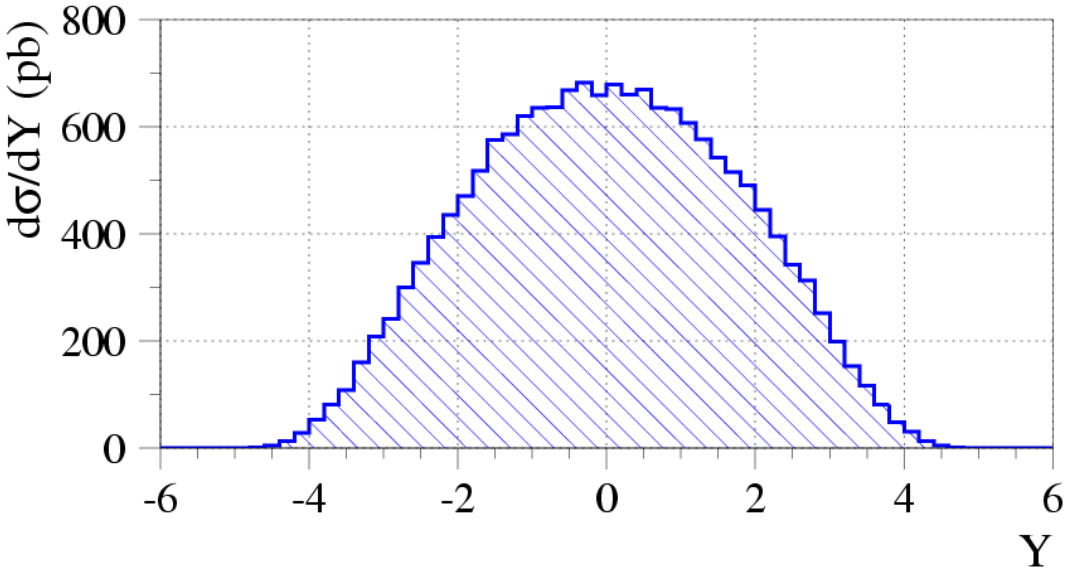

Figure 25: *normalized q_T distribution for the $\Upsilon(1s)$ from PYTHIA*

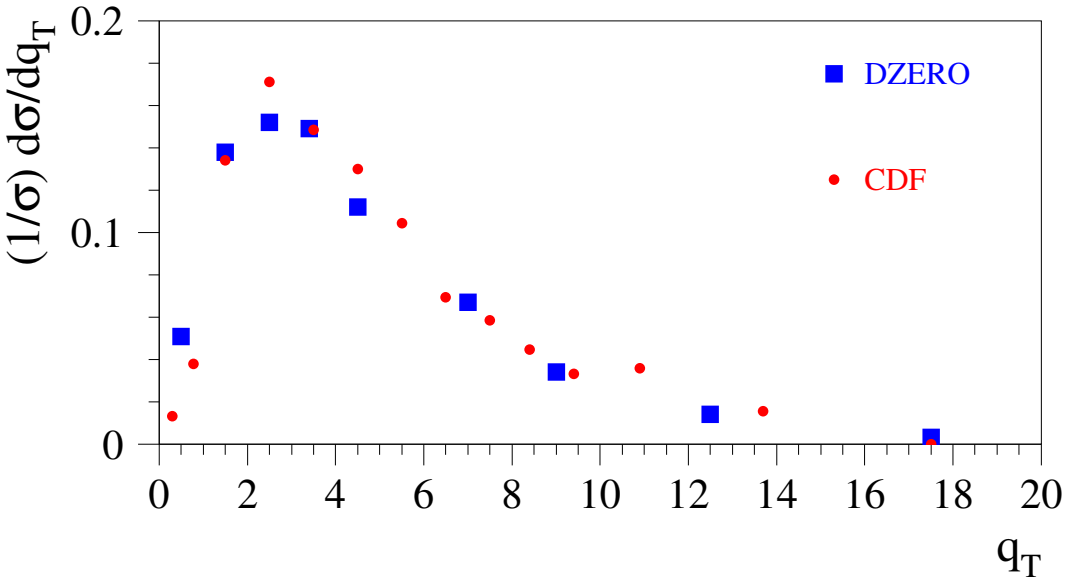

Figure 26: *normalized differential cross-sections $(1/\sigma)(d\sigma/dq_T)$ from the CDF Run I measurement (small circles) and the DØ Run II measurement (larger squares)*

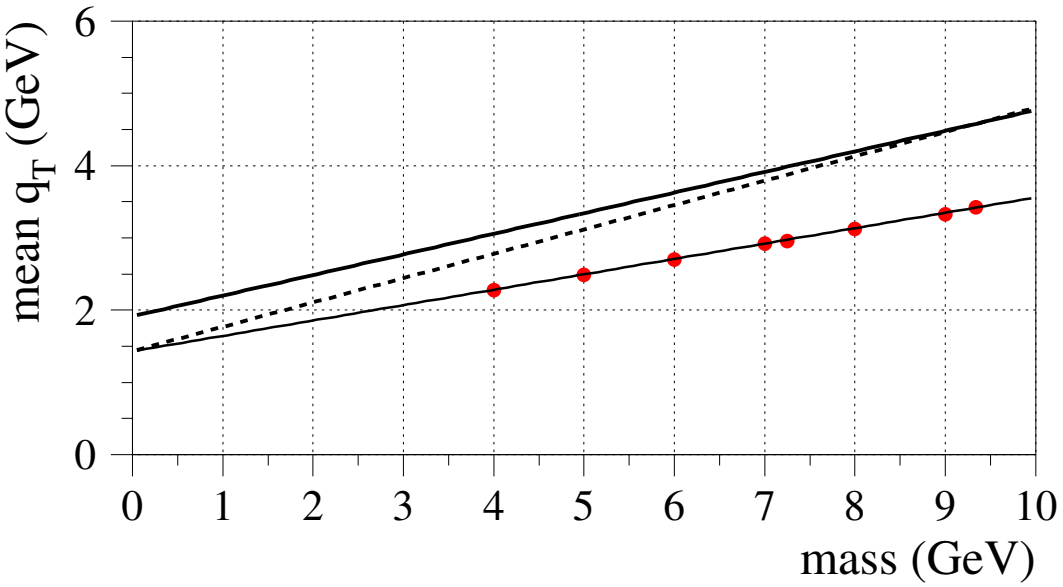

Figure 27: $\langle q_T \rangle$ *as a function of mass. Lower solid line with points shows straight PYTHIA. Upper solid line shows the PYTHIA curve scaled by the ratio of* $\langle q_T \rangle$ *for CDF data and PYTHIA. The dashed line shows a linear curve which passes through the CDF measurement at* $M_{\mu\mu} = M(\Upsilon)$*, and the PYTHIA value at zero.*

where, clearly, $\langle q_T \rangle = 3.42$ GeV for the $\Upsilon(1s)$ in PYTHIA (for all rapidity). Our guess as to how the true $\langle q_T \rangle$ evolves is obtained by scaling the values from Eq. (8) by the ratio of true $\langle q_T \rangle = 4.58$ GeV (from the CDF measured cross-section) to the PYTHIA value. We show this in Fig. 27 as the upper solid line. The PYTHIA behavior is the lower solid line with the dots.

It is interesting that the PYTHIA curve suggests $\langle q_T \rangle \approx 1.4$ GeV for zero mass. This may arise from a non-perturbative effect, such as the intrinsic-k_T of the partons inside the proton, of some sort of transverse momentum scale associated with gluon radiation. It may be that that value is fundamental, so we construct an alternative hypothesis for $\langle q_T \rangle$ as a function of mass, which is a straight line passing through the CDF value on the $\Upsilon(1s)$ and that value ≈ 1.4 GeV at zero. This is shown as the dashed line in Fig. 27.

We summarize our values for the acceptance in Table 2 and display them in Fig. 28. The table also lists the acceptance predicted for Drell-Yan like processes, and also for the alternative hypothesis given by the dashed line in Fig. 27.

6.3 Systematic Uncertainties

All of the systematic uncertainties enter with the calculation of the limits on the cross section from the limits on the number of signal events. We consider the following:

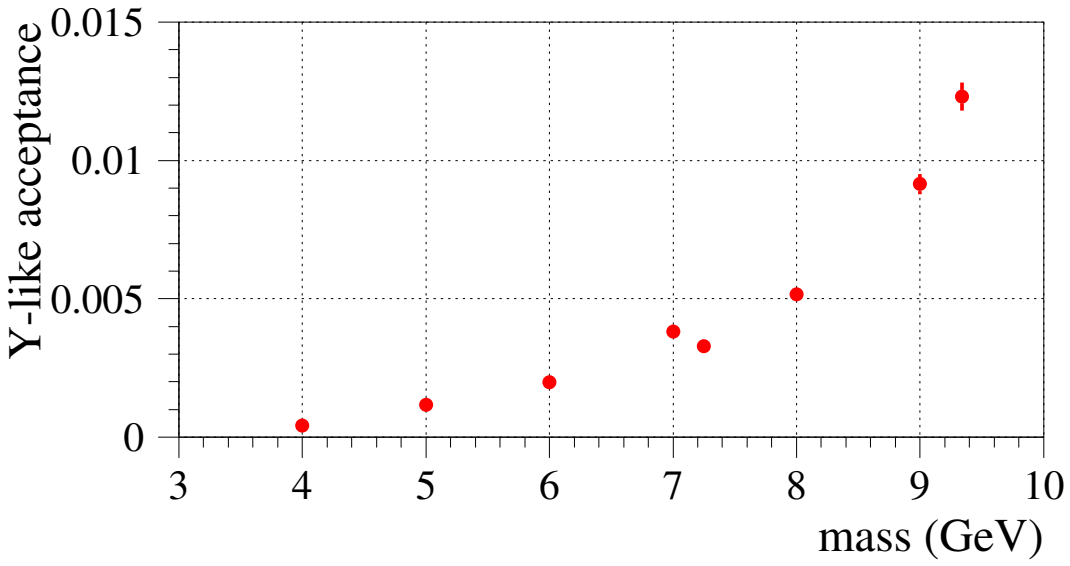

Figure 28: *acceptance for* Υ*-like objects as a function of mass*

mass (GeV)	Drell-Yan–like	Υ–like PYTHIA	Υ–like best guess	Υ–like alternative
9.34	5.71	5.99 ± 0.25	12.31	12.31
9	4.60	3.92 ± 0.20	9.15	9.08
8	2.44	1.56 ± 0.12	5.16	5.02
7.25	1.51	0.74 ± 0.09	3.28	3.10
7	1.29	0.76 ± 0.09	3.81	3.50
6	0.68	0.33 ± 0.06	1.98	1.45
5	0.36	0.15 ± 0.04	1.17	0.86
4	0.19	0.02 ± 0.01	0.43	0.12

Table 2: *acceptance as a function of mass. All numbers are* $\times 10^{-3}$

- mass-dependence of the efficiency
- mass-dependent uncertainties on the acceptance (under our given premise that the acceptance for the signal coincides with that for Drell-Yan di-muon production)
- the mass resolution
- the uncertainty on the overall normalization

At present we have an approximate evaluation for these uncertainties, as we now describe. We will work to refine these evaluations later as we expand the data sample.

We devised the sliding cuts on ΔX and the isolation in order to reduce the p_T-dependence of the efficiency. As shown Ref. [7], this works very well down to a $p_T = 10$ GeV, and we expect it is good down to $p_T = 5$ GeV at the level of 5% or better. As a check that the simulation is not very wrong for ΔX, we show this quantity for data and simulated Drell-Yan events in Fig. 29 for the CMP and CMX, for two ranges of muon p_T. The agreement is quite good. We assign an uncertainty of 0.02 for $M_{\mu\mu} > 10$ GeV, and a rising uncertainty at lower masses: $0.02 - 0.01(M_{\mu\mu} - 10\ \text{GeV})$.

The mass resolution was investigated in some detail in Ref. [7]. By considering extreme modifications in the parametrization of the mass resolution, the expected yields changed by $< 3\%$. The main issue there was the feed-down of the Z-peak into the lower-mass regions, which is of no concern for the present analysis. Since the first version of this note, we have more carefully described the mass resolution for $M_{\mu\mu} < 14$ GeV where the requirement $p_T > 5$ GeV begins to make a difference. Our study reproduces well the observed widths of the $\Upsilon(1s)$ and J/ψ resonances. We assign an uncertainty of 3% for all masses.

The acceptance uncertainty would come mainly from the PDF's, and simulation of the q_T distribution. We have evaluated both in Ref. [7] down to $M_{\mu\mu} = 20$ GeV and also verified carefully the generator-level mass distribution of the γ^*/Z's by comparing PYTHIA to RESBOS [10] and PHOZPRMS [11]. On this basis we would assign a PDF uncertainty of 0.02 for $M_{\mu\mu} > 14$ GeV and a rising uncertainty $0.02 - 0.004(M_{\mu\mu} - 14\ \text{GeV})$ for lower masses.

For the case of Υ-like objects, there are additional significant uncertainties coming from the strong bias in q_T and the lack of knowledge of the differential cross-section. We varied the parameterizations of the acceptance function and found maximum excursions of 15%, so we assign that as a systematic. The propagation of the errors of the CDF Run I measurement contributes 4%. The comparison of the defaults model for $\langle q_T \rangle$ as a function of mass, and of the alternative model gives another systematic which is given by the ratio of the two relevant columns in Table 2. This is, for example, 40% for $M_{\mu\mu} = 5$ GeV. Finally, there is an uncertainty for the unknown polarization of a new vector state; this amounts to about 10% for the Υ and increases at lower masses. It is absent for a scalar state, of course.

Finally, there is some uncertainty in the overall normalization. The statistical uncertainty is only 1.7%. There is also the systematic uncertainty on the measured value of $\sigma(p\overline{p} \to Z \to$

$\ell^+\ell^-$), which is 2.2%, setting aside the error on the luminosity which cancels out. We assign an overall normalization uncertainty of 2.8%.

We add the contributions in quadrature as a function of mass. Above $M_{\mu\mu} = 20$ GeV all components are constant, and the total systematic uncertainty is 4.7%. In region 2 the total uncertainty us much larger and varies strongly with mass. A plot of the total and the main components is shown in Fig. 30.

To take systematics into account, we consider that we would normally convolute a Gaussian probability density function representing the total systematic uncertainty with the probability density function for the fitted amplitude, which is itself a Gaussian. The result would be analogous to a simple increase in the width of the original Gaussian for the amplitude from σ_a to $\sigma_a \times (1 + \kappa)$, where κ is the total relative uncertainty. Thus, when applying the Feldman-Cousins prescription, we simply take $X = a/[\sigma_a \times (1 + \kappa)]$ and then derive the corresponding limit on μ. The impact is quite small, of order κ or less.

6.4 The 4–9 Region

Armed with the Feldman-Cousins prescription and a preliminary estimate for the total systematic uncertainty, we can go ahead and derive the limits on the number of signal events, and on the signal cross section. The result is shown in Fig. 31.

The result here is, numerically, rather poor due to the very bad acceptance for the SUSY di-lepton trigger and our cut $p_T > 5$ GeV for mass states below $M_{\mu\mu} = 10$ GeV. This region could be greatly improved by using one the triggers implemented by the B-group.

6.5 The Υ Region

We derived limits on the numbers of signal events and signal cross section (still normalizing to the Z-peak) – see Fig. 32. The small fluctuation near $M_{\mu\mu} = 9.2$ GeV is evident in the excursion away from zero of the lower limits on the number of signal events and the cross section. However, this does not mean that a signal is present, as explained earlier in Sec. 6.1. There is no evidence for any new signal in this region.

6.6 The 13–84 Region

The limit plots for this region are shown in Fig. 33. The signal cross section generally must be below roughly 20 pb. We note for comparison that the Drell-Yan cross-section is much larger than this for most of this range.

6.7 The Z-peak Region

Fig. 34 shows the limits on the number of signal events and the signal cross section for this region. As expected they are quite weak given the huge background provided by the Z-peak

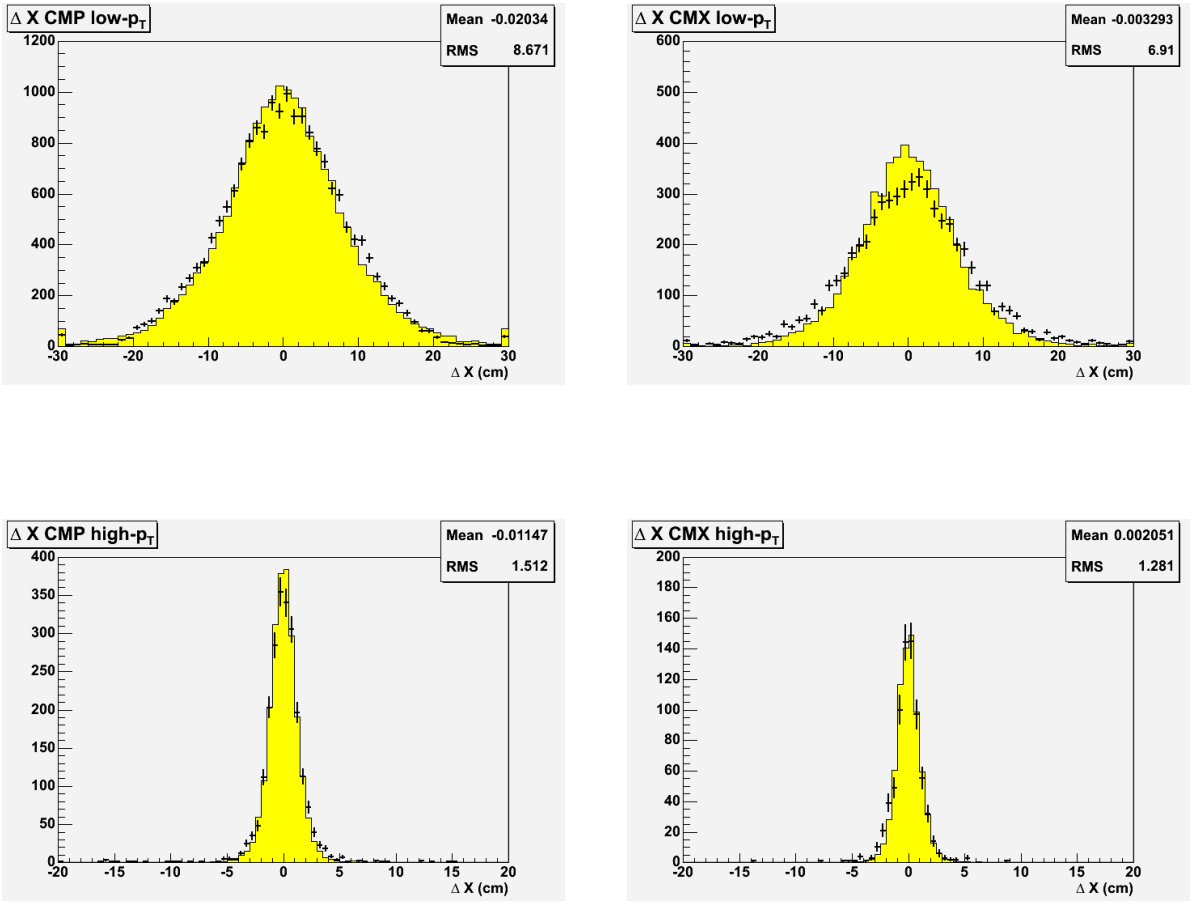

Figure 29: *muon matching quantity ΔX for the CMP (left) and the CMX (right), for $p_T <$* 10 GeV *(top) and $p_T >$* 20 GeV *(bottom). The points are data and the histogram, simulated Drell-Yan events.*

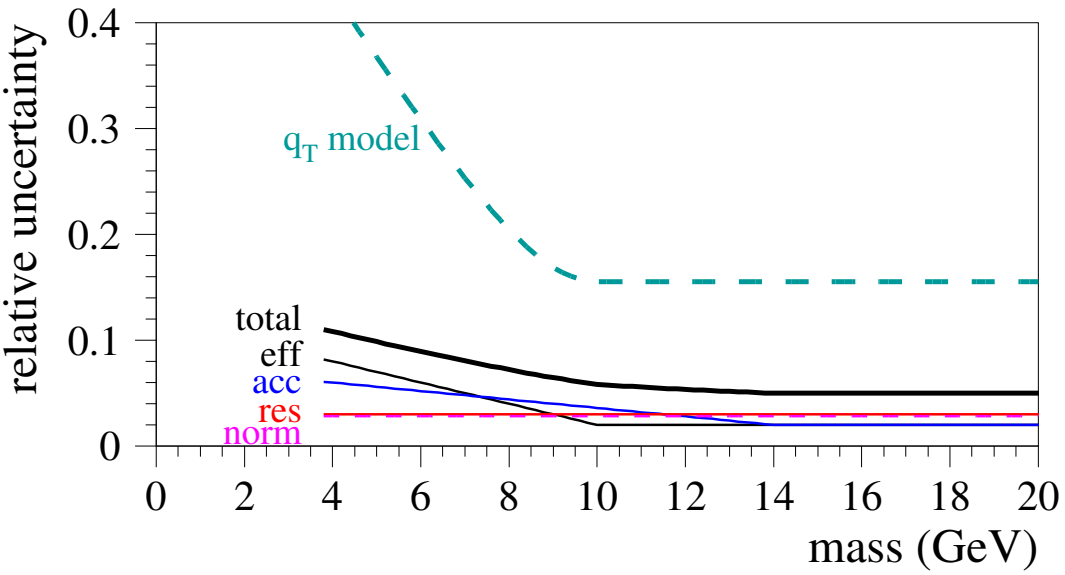

Figure 30: *relative systematic uncertainties as a function of mass. The components from efficiency, acceptance, mass resolution, and overall normalization are indicated. The total is the quadratic sum of all these. All components have a constant value above* $M_{\mu\mu} = 20$ GeV*. Also shown is the model uncertainty when assuming an* Υ*-like object.*

itself.

6.8 The High-Mass Region

The results for this region are shown in Fig. 35. Here we finally enter the regime of sub-pb cross sections. Toward the high end of the plot, the limit is about 200 fb.

7 The Specific Case $M_{\mu\mu} = 7.25$ GeV

G. Apollinari *et al.* published a report of evidence from Run I data for a new state decaying to opposite-sign muon pairs with a mass at $M_{\mu\mu} = 7.25$ GeV. They refer to it as a "fluctuation" but still quote a probability of 4.1×10^{-4} corresponding to 3.5σ.

William Wester queried the Run I data also, and found no statistically significant excess in the region 6.35 GeV $< M_{\mu\mu} <$ 9 GeV [12]. Thus the evidence for this new state was not firmly established with the Run I data.

With the much larger data sample available to us now, and with the improved tracking and muon systems, it is possible to probe this region again.

The conclusion of the Apollinari paper, which was published in Physical Review, includes

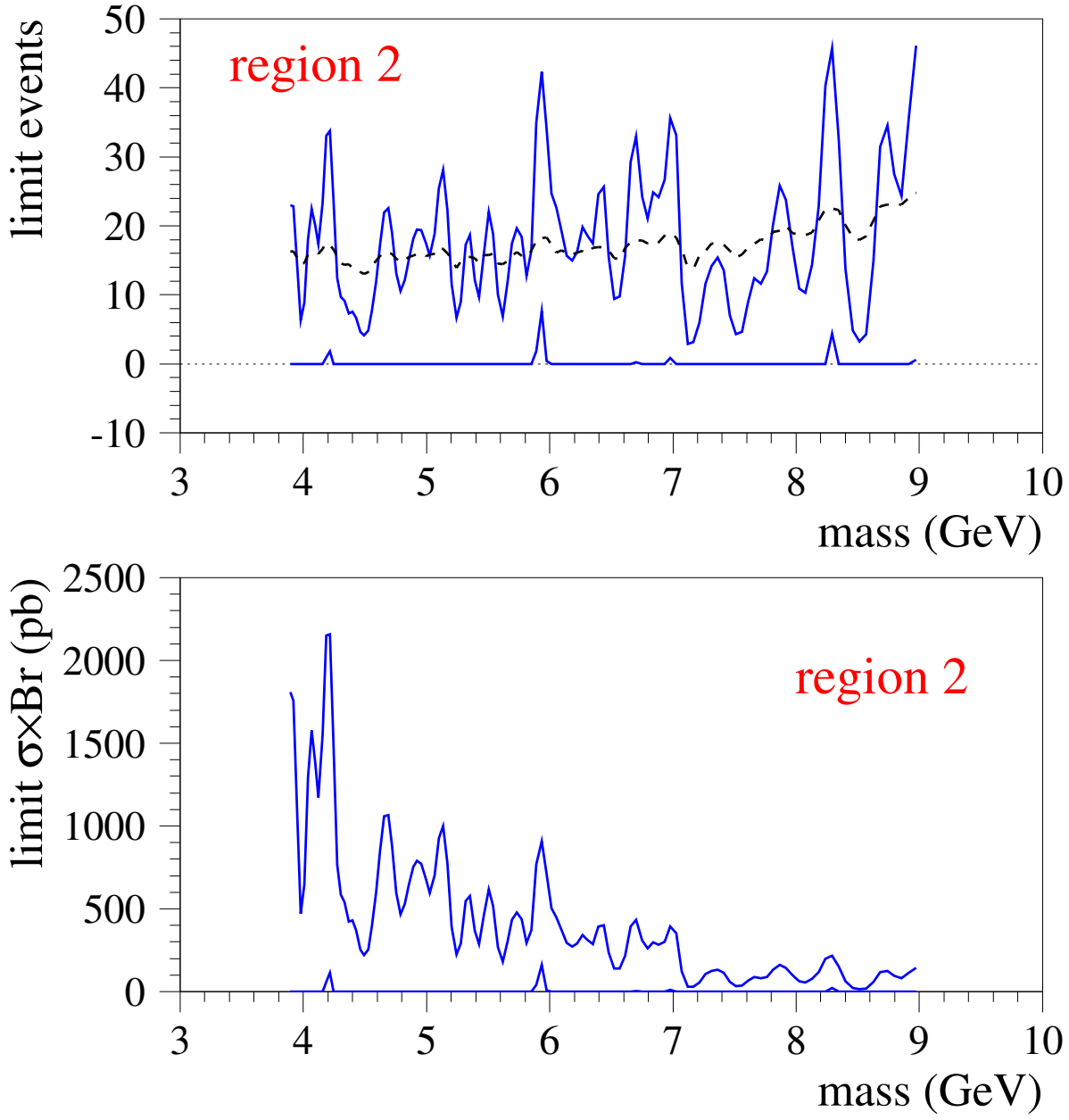

Figure 31: *limits for region 2. Top: limit on the number of signal events as a function of mass, based on the Feldman-Cousins prescription. Bottom: limit on the signal cross section. The dashed lines show the expected limit in the absence of signal.*

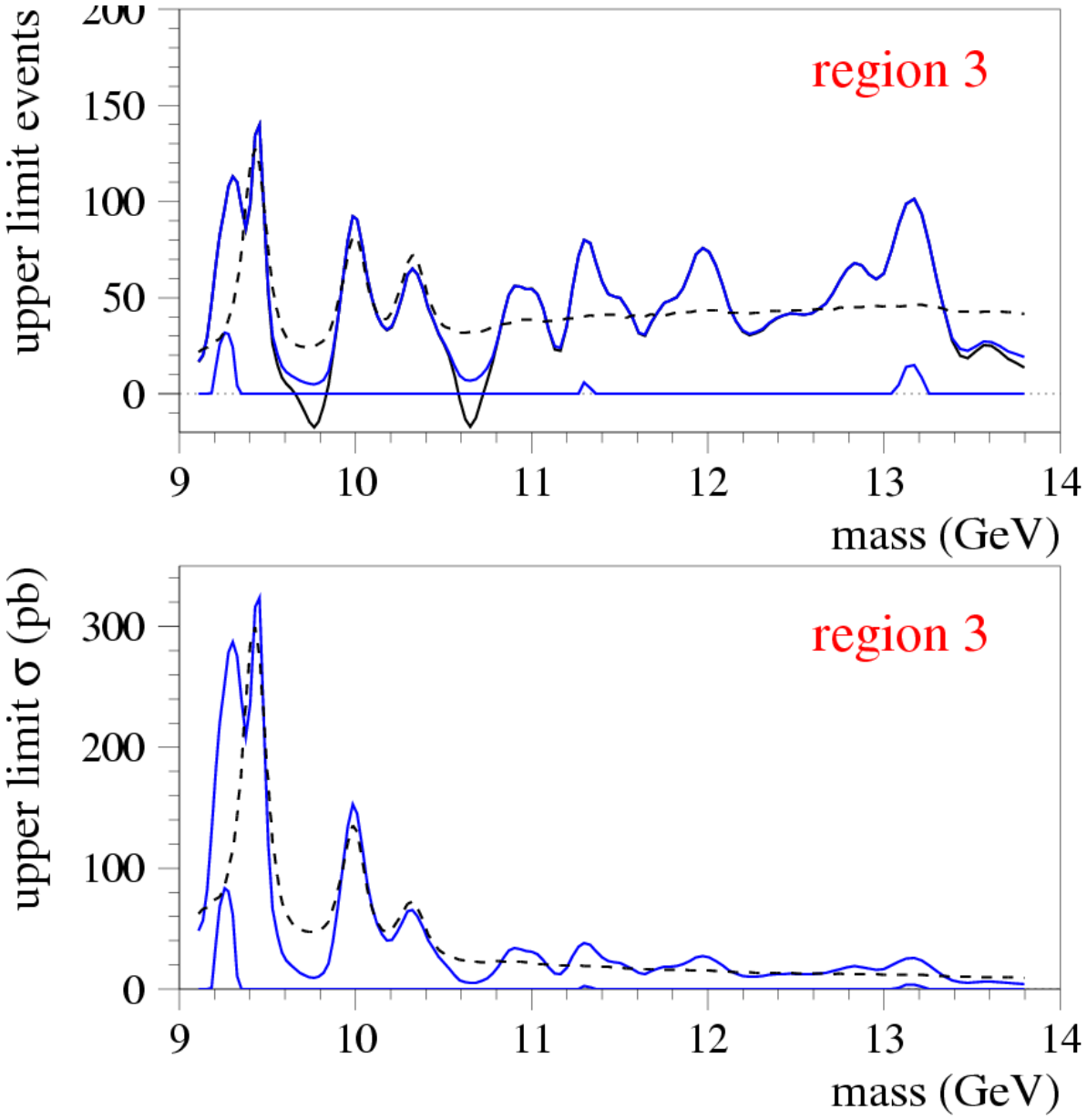

Figure 32: *limits for region 3. Top: limit on the number of signal events as a function of mass, based on the Feldman-Cousins prescription. Bottom: limit on the signal cross section. The dashed lines show the expected limit in the absence of signal.*

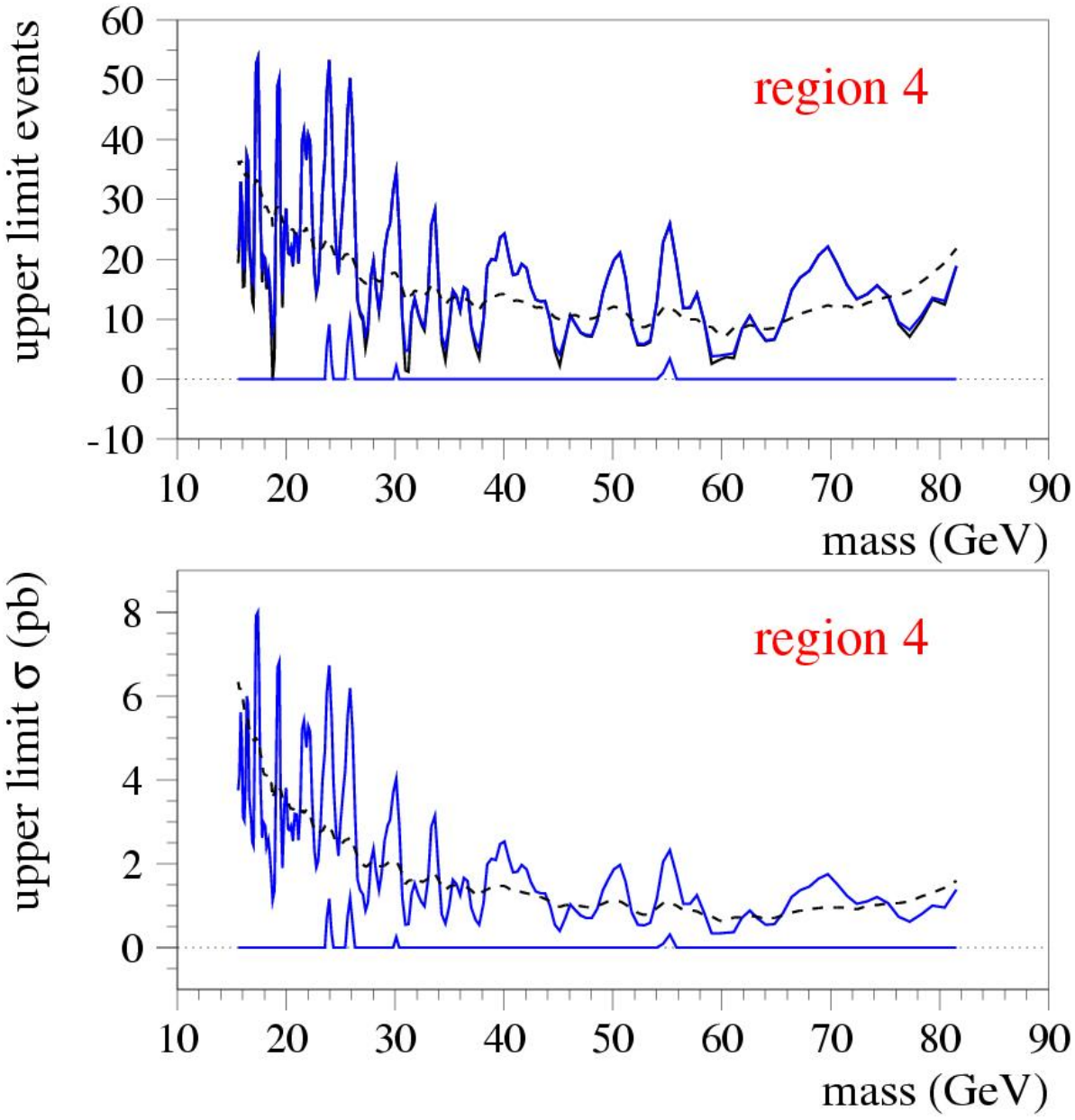

Figure 33: *limits for region 4. Top: limit on the number of signal events as a function of mass, based on the Feldman-Cousins prescription. Bottom: limit on the signal cross section. The dashed lines show the expected limit in the absence of signal.*

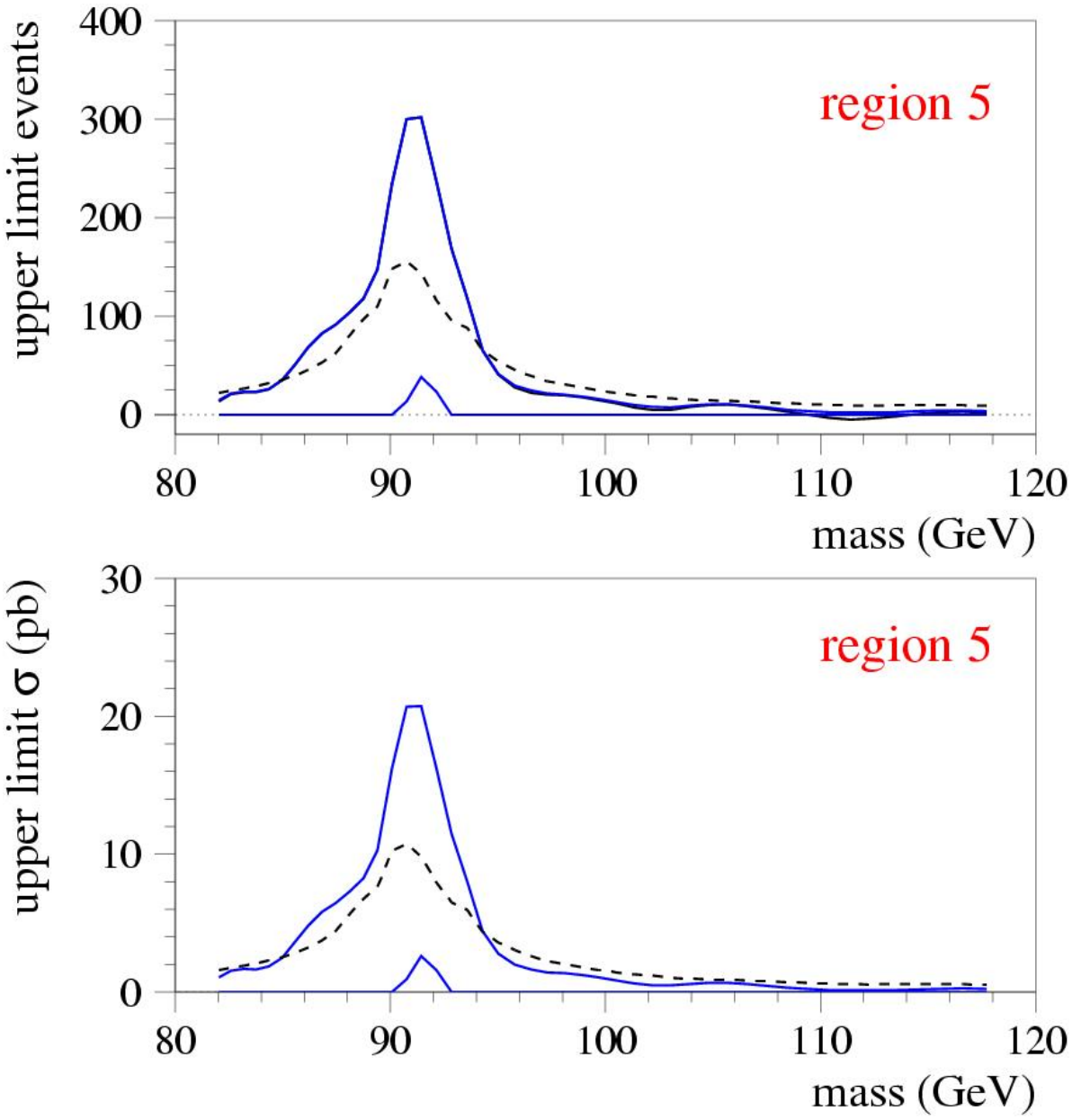

Figure 34: *limits for region 5. Top: limit on the number of signal events as a function of mass, based on the Feldman-Cousins prescription. Bottom: limit on the signal cross section. The dashed lines show the expected limit in the absence of signal.*

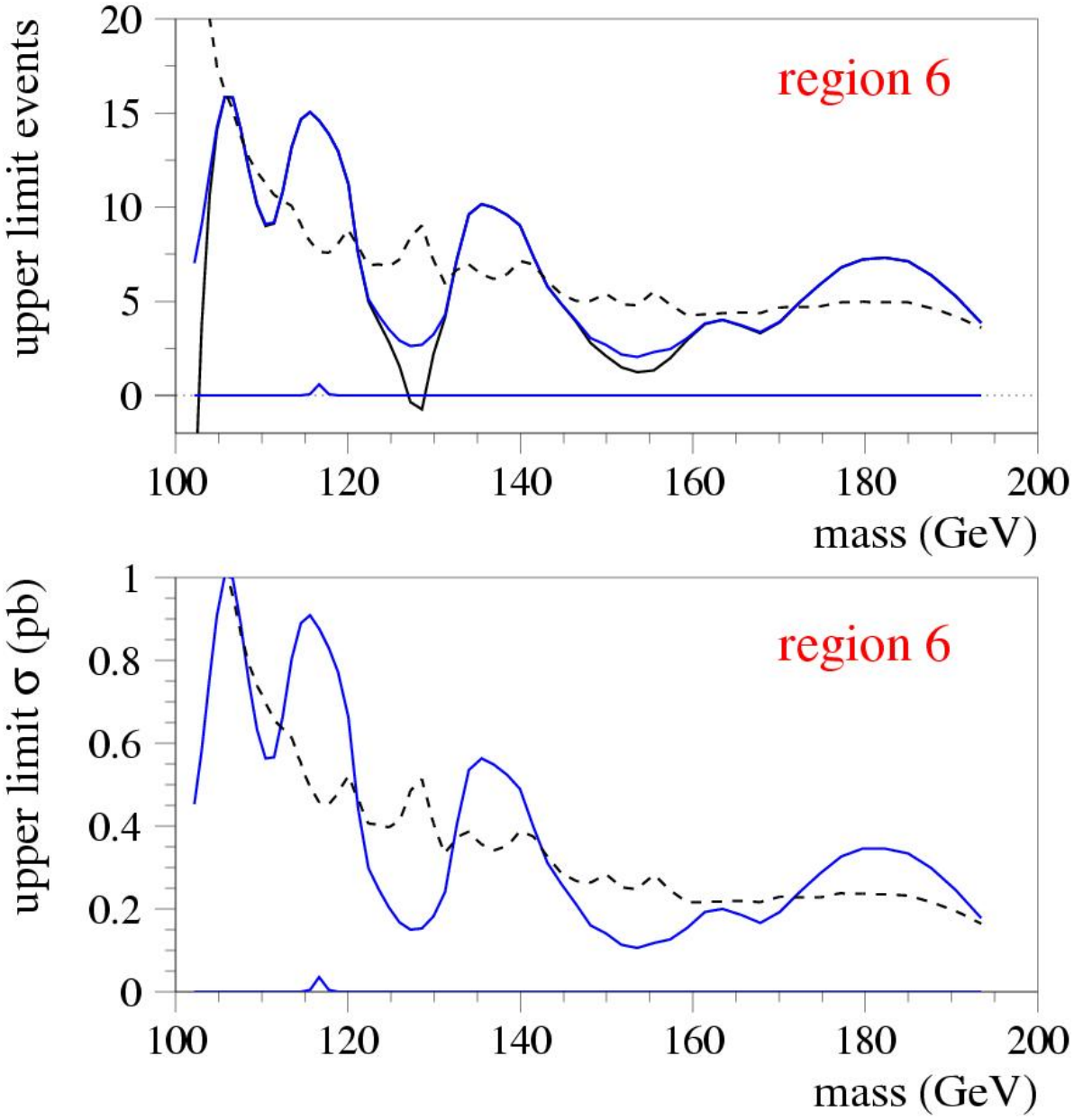

Figure 35: *limits for region 6. Top: limit on the number of signal events as a function of mass, based on the Feldman-Cousins prescription. Bottom: limit on the signal cross section. The dashed lines show the expected limit in the absence of signal.*

the statement that

$$\frac{\sigma_\varepsilon \times Br(\varepsilon \to \mu^+\mu^-)}{\sigma_{\Upsilon(1S)} \times Br(\Upsilon(1S) \to \mu^+\mu^-)} = (3.6 \pm 0.9)\% \tag{9}$$

where "ε" is their name for the state. There are two motivations for reporting their result in this form:

- the $\Upsilon(1S)$ resonance is close-by in mass, and therefore provides an appropriate normalization point. Furthermore, they optimized their quality cuts on the basis of the significance of their $\Upsilon(1S)$ signal.
- this paper discusses the possibility that the new ε state might be the bound-state of two down-type scalar quarks. Theoretical predictions for the production and decay of such a state can safely be related to the Υ.

We will therefore re-cast our limits in this region in terms of our yield of $\Upsilon \to \mu^+\mu^-$, though we have made no attempt at present to apply quality cuts to improve our $\Upsilon(1S)$ signal. We note in passing, however, that this Run II $\Upsilon(1s)$ signal is very clean (see Fig. 3) and stands on only half of the continuum than does the $\Upsilon(1s)$ signal published in the Apollinari paper. The cleanliness of our signal comes from demanding two "tight" muons. The Run I analysis used also stub-less muons, which helped avoid the strong q_T bias which is a difficult in this analysis.

Due to the strong q_T bias (see Fig. 23), we are forced to consider some model-dependence for our results, since the primary q_T distribution will vary from process to process. We can envision three realistic models:

1. Drell-Yan–like production, such as would be expected for a very light neutral gauge boson of some sort,
2. Υ–like production, such as would be appropriate for a bound state of two quarks or two squarks; and,
3. a light state which is produced in the decay of a heavier one: $p\overline{p} \to AX$ with $A \to BY$ and $B \to \mu^+\mu^-$ where it is the B particle that we observe.

At this time we do not address the third possibility. We believe the first one to have the poorest acceptance in region 2, and the second to have somewhat better acceptance, and the third, much better acceptance.

According to this analysis, the upper limit on the number of events at $M_{\mu\mu} = 7.26$ GeV is 11.6 events (see Fig. 31). Indeed, let's first check this number by opening a window of $\pm 3\sigma$ about $M_{\mu\mu} = 7.25$ GeV and counting the number of events. (Since $\sigma_M = 0.049$ GeV at $M_{\mu\mu} = 7.25$ GeV, this window is $7.104 < M_{\mu\mu} < 7.396$ GeV.) We count $N_{\rm obs} = 114$ events, and from the continuum parametrization, we expect $N_{\rm exp} = 135$ events. Thus there is a

downward fluctuation at this mass value. The one-sided 95% CL upper limit corresponds to $1.645\sigma = 19.1$ events. However, since the data have fluctuated downward, the upper limit from these data is lower, namely 11.6 events. If we were not using the Feldman-Cousins prescription, then the upper limit would be much lower than this.

Consider the Υ–like model first. In this case the acceptance is estimated to be $A(7.25) = 3.28 \times 10^{-3}$ and $A(9.34) = 12.31 \times 10^{-3}$ (see Table 2). The upper limit on the ratio of cross-section is, then,

$$\frac{\sigma \times Br(\varepsilon)}{\sigma \times Br(\Upsilon)} < \left(\frac{11.6}{3134}\right) \times \left(\frac{12.31 \times 10^{-3}}{3.28 \times 10^{-3}}\right) = 0.014. \tag{10}$$

This is a little bit "lucky" due to the downward fluctuation in the data; the expected limit would be 0.023. These numbers ignore systematics, however. Referring to Fig. 30, we see that the the systematic uncertainty for $M_{\mu\mu} = 7.25$ GeV is 24% for the q_T model, on top of 8% for all other systematics; adding this in quadrature gives 25%. Much of this systematic uncertainty would cancel in the ratio in Eq. (10), but we will ignore that fact. Furthermore, the convolution of a Gaussian uncertainty of width 0.25 amounts to a modest effect, but to be very conservative we will simply downgrade our result by 25%, and obtain

$$\frac{\sigma \times Br(\varepsilon)}{\sigma \times Br(\Upsilon)} < 0.018 \qquad \text{at 95\% CL} \tag{11}$$

for the case in which the ε particle is produced in a manner similar to the Υ. The expected limit is 0.029. A plot of the ratio in Eq. (11) as a function of mass is given in Fig. 37. We remind the reader that there is evidence discussed earlier that our acceptances may be underestimated, which if corrected would lead to stricter bounds than these. These results, with this model under consideration, do not confirm the measurement by Apollinari *et al.* in Eq. (9).

We now consider the case of Drell-Yan–like production. We must first convert the Run I result into a cross-section, which we do as follows: Numerically, Eq. (9) leads to $d\sigma(\varepsilon)/dy = 24$ pb, based on the Run I measurement of $\Upsilon(1s)$ production [8]. We integrate this now over the *Drell-Yan* rapidity distribution from PYTHIA (Fig. 36), and obtain

$$\sigma \times Br(\varepsilon \to \mu^+\mu^-) = 201 \pm 50 \text{ pb} \tag{12}$$

to be compared to the upper limit we obtained from the data:

$$\sigma \times Br(\varepsilon \to \mu^+\mu^-) < 114 \text{ pb} \qquad \text{at 95\% CL} \tag{13}$$

where again, we have degraded our limit by the total systematic uncertainty of 8%. Also in this case, the observation of Apollinari *et al.* is not confirmed.

Finally, we filled a histogram with the data so that it can be compared to the distribution published by Apollinari *et al.* – see Fig. 38.

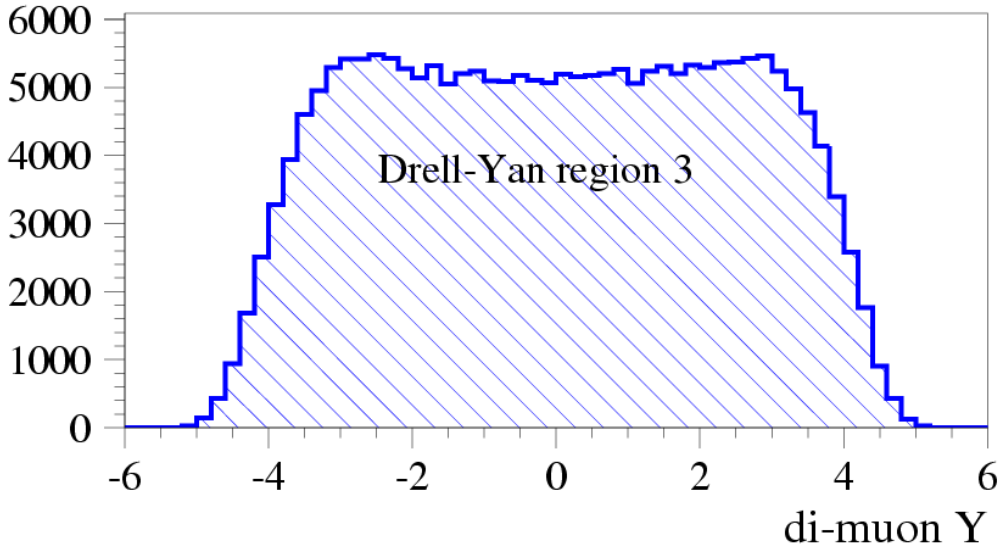

Figure 36: *PYTHIA-generated rapidity distribution for Drell-Yan events in the* Υ *region*

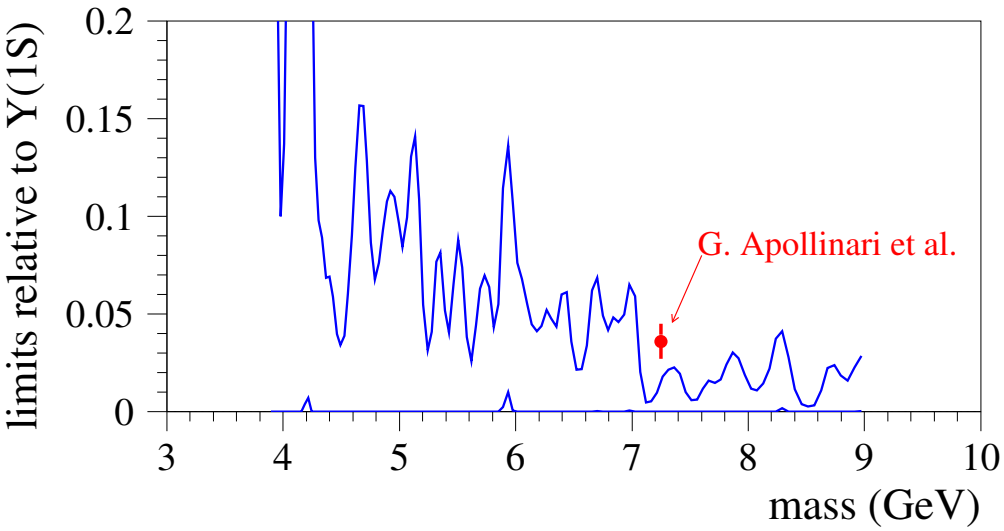

Figure 37: *limits on the ratio of cross-sections. The measurement reported by Apollinari* et al. *is also indicated.*

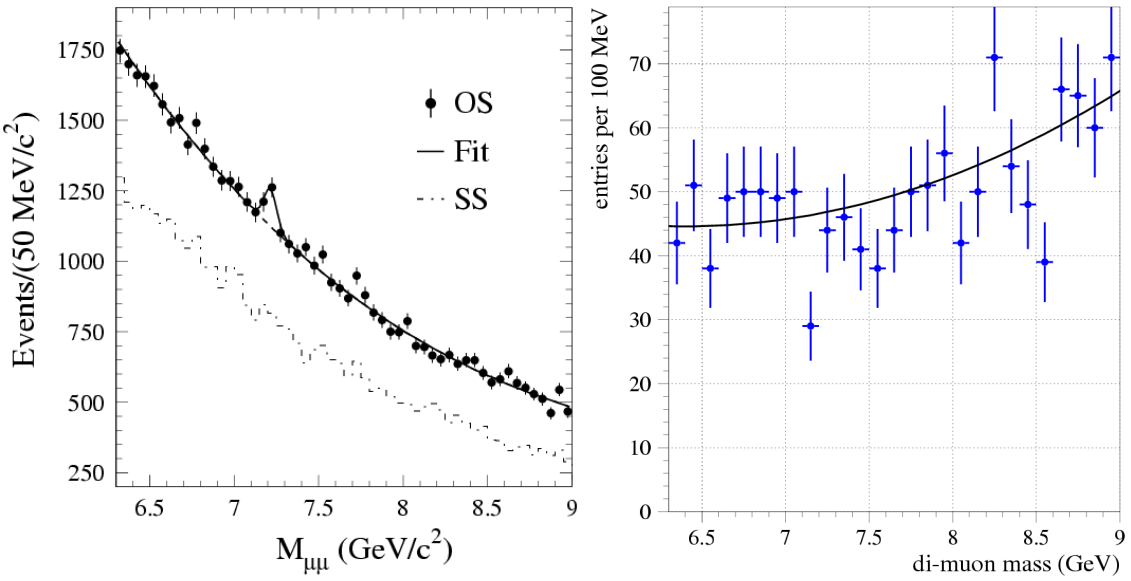

Figure 38: *comparison of the di-muon mass spectrum published by Apollinari* et al. *(left), and from this analysis (right)*

We would like to emphasize that the limits we have produced are model-dependent. We have taken up two examples which we believe are physically reasonable, and we have tried to make reasonable estimations of systematic uncertainties and have injected conservatism in various ways. Nonetheless, it may be true that some other model produces a peak at $M_{\mu\mu} = 7.25$ GeV for which we have little sensitivity; in this sense our results cannot be said to be definitive except within the stated models. If someone is able to devise a realistic model in which the q_T spectrum is softer, then we would like to attempt to estimate our sensitivity for that model.

8 The Case of Sparse Data

The key element of this analysis is the *shape* of the mass distribution – whether there is a peak on top of a smooth continuum or not. When we extend our investigations into the highest mass region, however, we will not be able to parametrize the continuum any longer. Also, this is not the region in which one can be certain of Monte Carlo predictions. Nonetheless, we can still key in on the *shape* of whatever sparse distribution we see.

Suppose we observe $N = \mathcal{O}(10)$ events past the point where the parametrization for the high-mass region predicts more than a couple of events. Distinguish two cases:

1. the events are distributed flatly.

2. the events are clumped together, like a Gaussian.

We will not consider the case where some events are from a flat distribution and the others are Gaussian – we want to test these two hypotheses.

It is pessimistic and probably unrealistic to assume that the continuum is flat. One could instead use the fit from the high-mass channel. However, there could be a background, such as cosmic rays, or poorly-reconstructed events, which appear only once the real Drell-Yan events have petered out. Thus using the fit from the high-mass channel would be optimistic, and potentially quite wrong. On the other hand, it is not at all likely that the continuum mass distribution *increases* with mass.

In making the assumption of a flat continuum, and following the procedure specified below, we give away some important information: the prediction of the number of events, and the observation. One could quantify that probability (with whatever substantial systematic uncertainty attaches to the prediction), and consider it separately or in addition to the probability to be derived from the shape (flat *vs.* clumped) alone.

It should be kept in mind that one would not perform the following shape analysis unless there were a surprising number of events observed.

We need to define our mass range for investigating the distribution: is it flat or clumped?. The lower point can be defined by the parametrization of the high-mas region. For example, $x_{\rm LO}$ could be the point beyond which the extrapolation of the fitted continuum would give one event or fewer. The upper point is more difficult to choose. It turns out that the more 'conservative' choice is to take it as low as possible. So we take $x_{\rm HI}$ to be the mass of the highest-mass event.

Given N events in the range $x_{\rm LO} < x < x_{\rm HI}$ with mass values x_i, we order them in increasing mass, and then compute the $N-1$ intervals $d_i \equiv x_{i+1} - x_i$. Clearly one expects the typical interval for x_i from a flat distribution to be characteristically larger than for a clumped distribution. This can be quantified by constructing two probabilities: P_F, the probability to observe the given $N-1$ values $\{d_i\}$ if the underlying distribution for the N measurements $\{x_i\}$ is flat, and P_G, the corresponding probability if they are Gaussian.

Our test statistic will be based on the ratio of these probabilities:

$$S \equiv -\ln(P_G) + \ln(P_F). \tag{14}$$

This will tend to be positive if the masses come from a Gaussian distribution, and negative if they come from a flat distribution.

In order to illustrate these ideas, we ran a toy simulation with $N = 10$. We set $x_{\rm LO} = 200$ GeV, and compared a truly flat distribution to a Gaussian with $x_{\rm PK} = 750$ GeV, which gives $\sigma_M = 90$ GeV. The distribution of intervals is exponential to a good approximation. For a flat distribution, the correct parameter λ (as in Eq. (4)) is simply $(x_{\rm HI} - x_{\rm LO})/N$. For the Gaussian distribution, we found the correct λ by Monte Carlo methods. The comparison of these two interval distributions is given in Fig. 39.

How well can flat and clumped distributions be distinguished with this test statistic, S? We simulated a thousand pseudo-experiments to form the distribution of S for a flat and for a Gaussian distribution, in order to get the distribution for S in both cases. Fig. 40 shows

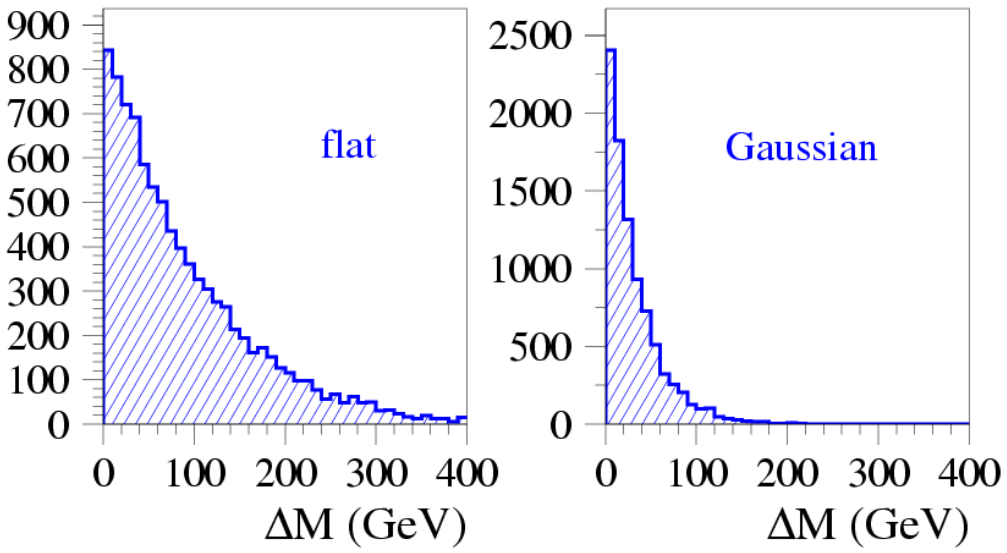

Figure 39: *comparison of distributions of intervals obtained for the toy Monte Carlo simulation*

the result: S is peaked toward 9 for the Gaussian distributions, and toward -4 for the flat distributions. The overlap of the two distributions is quite small, so these two hypotheses could be cleanly distinguished in this case.

We have not yet revealed what the real data hold for $M_{\mu\mu} > 200$ GeV. Once this procedure for "sparse data" has been discussed in the relevant CDF meetings, we will proceed.

9 Summary and Conclusions

We have developed a new method to look for narrow peaks in the di-muon mass spectrum recorded by the CDF experiment. This method has been applied to about 195 pb^{-1} of data recorded with the SUSY di-lepton trigger. We divided the mass spectrum in several regions, which together span the range $4 < M_{\mu\mu} < 200$ GeV. We see no evidence for any peaks in this range, and have derived limits on the signal cross section using the Feldman-Cousins procedure.

We put together all cross section limits – in correspondence of our original goal – and plotted them at once in Fig. 41. The limit can be compared to the theoretical cross-section obtained with program PHOZPRMS [11].

The region above $M_{\mu\mu} = 200$ GeV cannot be addressed with this procedure, so we suggest a second procedure appropriate for "sparse" data. We have illustrated how this procedure would work, but we have not yet applied it to the data.

Much more data have been recorded by CDF, and we are preparing to analyze it with

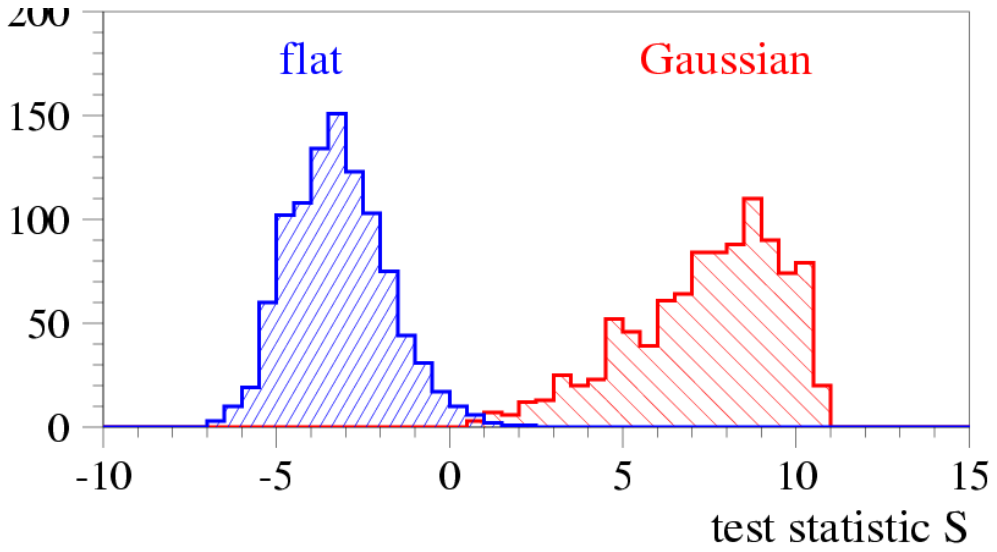

Figure 40: *distribution of the test statistics S for events from a flat distribution and from a Gaussian. The two cases could be clearly distinguished in this toy example.*

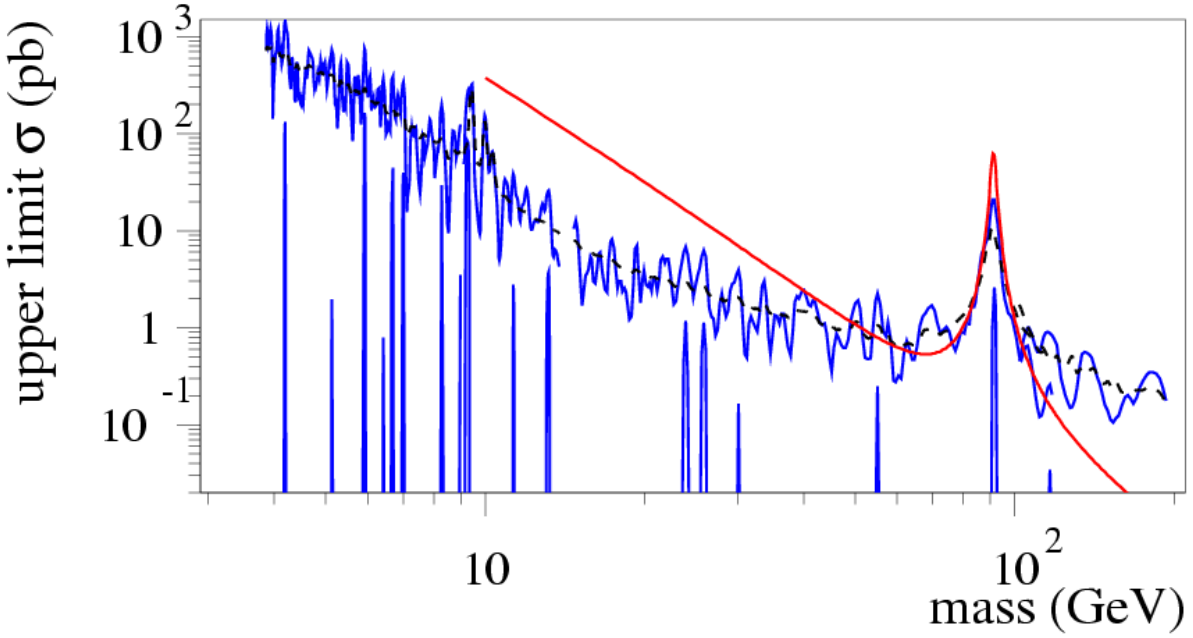

Figure 41: *cross-section limits for all regions. The solid red line shows the theoretical Drell-Yan cross section.*

the methods described in this note.

10 Version History

`version 0:` March 20, 2006. Original version posted to the web.

`version 1:` April 19, 2006. Update and improve understanding of mass resolution (relevant for region 2). Include studies comparing generator-level simulations, full simulations, and data. Discussion of non–Drell-Yan backgrounds as estimated with the same-sign events. Discussion of $\Upsilon(1s)$ yield and acceptance as a function of q_T. More complete treatment of systematics. More detailed discussion of the ε case.

References

[1] G. Apollinari *et al.*, *Search for Narrow Resonances Below the Upsilon Mesons,* Phys.Rev. **D72** (2005) 092003 [Physical Review Online] [arxiv:hep-ex/0507044]

[2] discovery of the Υ:
S.W. Herb *et al.*, *Observation of a di-Muon Resonance at* 9.5 GeV *in* 400 GeV *proton–nucleus Collisions,* Phys. Rev. Lett. **39** (1977) 252
For fun, see also the relevant web pages from the [Fermilab History and Archives Project].

[3] Gary J. Feldman and Robert D. Cousins, *A Unified Approach to the Classical Statistical Analysis of Small Signals*, Phys.Rev. **D57** (1998) 3873 [Physical Review Online] [arxiv:physics/9711021]

[4] CDF Collab., *First Measurements of Inclusive W and Z Cross Sections from Run II of the Tevatron Collider,* Phys.Rev.Lett. **94** (2005) 091803. [Physical Review Online] [arxiv:hep-ex/0406078]

[5] cdf notes from the New Mexico group:
cdf6717: Vladimir Rekovic and Michael Gold, "Validation of the di-Lepton Data Set for SUSY Searches;"
cdf7096: Vladimir Rekovic and Michael Gold, "Validation of the di-Lepton Data edil0d Set for SUSY Searches;"
cdf7210: Vladimir Rekovic and Michael Gold, "Low-p_T Muon ID Efficiencies and Scale Factors for Exotics Searches"

[6] CDF Collab., *Search for New High Mass Particles Decaying to Lepton Pairs in $p\bar{p}$ Collisions at $\sqrt{s}$ = 1.96 TeV*, Phys.Rev.Lett. **95** (2005) 252001 [Physical Review Online] [arxiv:hep-ex/0507104]

[7] **cdf7560:** Jane Nachtman & Michael Schmitt, "Sliding-Q_T Ratio – Muon Channel"

[8] CDF Collab., "Υ Production and Polarization in $p\bar{p}$ Collisions at $\sqrt{s} = 1.8$ TeV," Phys.Rev.Lett. **88** (2002) 161802

[9] DØ Collab., "Measurement of Inclusive Differential Cross Sections for $\Upsilon(1s)$ Production in $p\bar{p}$ Collisions at $\sqrt{s} = 1.96$ TeV," Phys.Rev.Lett. **94** (2005) 232001

[10] references for the program RESBOS:
Csaba Balazs, Jian-wei Qiu and C.P. Yuan, *Effects of QCD Resummation on Distributions of Leptons from the Decay of Electroweak Bosons,* Phys. Lett. **B355** 548 (1995);
Csaba Balazs and C.P. Yuan, *Soft Gluon Effects on Lepton Pairs at Hadron Colliders,* Phys. Rev. **D56** 5558 (1997);
The code can be downloaded from the [official RESBOS web page].

[11] references for the program PHOPRMS:
R. Hamberg, W.L. van Neerven and T. Matsuura, *A Complete Calculation of the Order α_s^2 Correction to the Drell-Yan K-Factor,* Nucl. Phys. **B359** 343 (1991); Erratum *ibid.* **B644** 403 (2002)
The code can be downloaded from the web page of [Prof. dr. W.L. van Neerven].

[12] **cdf5390:** William Wester, "Search for a Prompt Narrow Resonance in Mass($\mu^+\mu^-$) between the J/ψ and $\Upsilon(1s)$"